Biophysical Investigation of G-Quadruplex Recognition by the N-Terminal Construct of RNA Helicase Associated with *AU*-Rich Element (RHAU)

by

Oksana Marushchak

A Thesis submitted to the Faculty of Graduate Studies of

The University of Manitoba

in partial fulfillment of the requirements of the degree of

MASTER OF SCIENCE

Department of Chemistry

University of Manitoba

Winnipeg, Manitoba, Canada

Abstract

G-quadruplexes, characterized by stacked G-tetrad rings held together by Hoogsteen hydrogen bonds, have been visualized in human cells and implicated in transcriptional and translational control, telomere maintenance and disease. RHA Helicase associated with *AU*-rich element (RHAU), a DEAH-box helicase, is a major G-quadruplex resolvase in human cell lysates. It binds G-quadruplexes through the RHAU specific motif in its N-terminus. In order to investigate the recognition of G-quadruplexes by helicases, the binding between the N-terminal construct of RHAU, $RHAU_{53\text{-}105}$, and the DNA analog of the quadruplex formed by the 5' terminus of human telomerase RNA component, $hTR_{1\text{-}20}$, was investigated in a comprehensive biophysical approach followed by crystallization screening. $RHAU_{53\text{-}105}$, $hTR_{1\text{-}20}$ DNA and their complexes were analysed by gel electrophoresis, UV-visible spectroscopy, spectropolarimetry, dynamic light scattering and small angle X-ray scattering (SAXS). The findings reveal that $hTR_{1\text{-}20}$ DNA, separated in two conformations by size exclusion chromatography in the presence of potassium cations, assumes a disk-like parallel G-quadruplex secondary structure in solution. Far-UV circular dichroism spectra and SAXS demonstrate that $RHAU_{53\text{-}105}$ assumes an extended (D_{max} = 7.8 nm , r_G = 2.1 (±0.2) nm) and ordered conformation in solution. The analysis confirms the binding between $RHAU_{53\text{-}105}$ and each conformation of the $hTR_{1\text{-}20}$ DNA quadruplex. Circular dichroism spectra indicate the retention of quadruplex secondary structure in both $RHAU_{53\text{-}105}$·$hTR_{1\text{-}20}$ DNA_{c1} and $RHAU_{53\text{-}105}$·$hTR_{1\text{-}20}$ DNA_{c2} complexes. This analysis provides some insight into the interaction between G-quadruplexes and the N-terminal domain of RHAU and identifies 0.2 M sodium formate, 20 % (w/v) polyethylene glycol 3350 and 1.5 M sodium chloride, 10 % (v/v) ethanol as preliminary conditions for crystallization of the complex of $RHAU_{53\text{-}105}$ and $hTR_{1\text{-}20}$ DNA_{c2}.

Acknowledgements

I would like to thank Dr. Jorg Stetefeld, Dr. Markus Meier and Dr. Trushar Patel for their supervision, guidance and support. I would also like to extend my gratitude to Dr. Sean McKenna, Dr. Evan Booy and Dr. George Orriss for their assistance.

Many thanks also go to Matthew McDougall and Natalie Krahn for their friendship, advice and support. In addition, I would like to express my appreciation for financial assistance from the Department of Chemistry, Faculty of Science and Faculty of Graduate Studies at the University of Manitoba as well as the Manitoba Health Research Council.

Table of Contents

List of Tables

List of Figures

List of Copyrighted Material for which Permission was Obtained

Figure 1- Figure by G-quadruplex.jpg: Julian Huppert Jlh29 derivative work: Iridos (G-quadruplex.jpg) [CC-BY-SA-2.5 (http://creativecommons.org/licenses/by-sa/2.5)], via Wikimedia Commons.

Figure 1 appears on page 2.

Figure 14 –Reference circular dichroism spectra reproduced with permission from Elsevier.

Brahms, S., and Brahms, J. (1980) Determination of protein secondary structure in solution by vacuum ultraviolet circular dichroism. *J. Mol. Biol. 138*, 149–78

https://s100.copyright.com/CustomerAdmin/PLF.jsp?ref=0b0f703a-b81b-460b-b08a-b71b1f020827

Figure 14 appears on page 43.

Figure 16 – Reproduced with permission from Journal of Biological Chemistry.

http://www.jbc.org/site/misc/Copyright_Permission.xhtml

Meier, M., Patel, T. R., Booy, E. P., Marushchak, O., Okun, N., Deo, S., Howard, R., McEleney, K., Harding, S. E., Stetefeld, J., and McKenna, S. a. (2013) Binding of G-quadruplexes to the N-terminal recognition domain of the RNA helicase associated with AU-rich element (RHAU). *J. Biol. Chem. 288*, 35014–27.

Figure 16 appears on page 45.

1. Introduction

1.1 G-QUADRUPLEX SECONDARY STRUCTURE OF OLIGONUCLEOTIDES

Oligonucleotides possessing consecutive stretches of three or more guanine bases can self-assemble into G-quadruplexes. These thermodynamically stable secondary structures result from stacking of planar guanine tetrads that form when four quinine bases associate in a ring-like structure through Hoogsteen hydrogen bonds (Figure 1). A central monovalent cation, usually potassium, sodium or lithium, is present in a central ion channel, stabilizing the quadruplex. Quadruplex structures with central cation positioned in line with the G-tetrads or in bi-pyramidal arrangement with successive G-tetrads have been reported.[1–4] Melting temperatures around 80º C have been reported for G-quadruplexes synthesized *in vitro*.[5–7]

Strand orientation, conformation of glycosidic angles of guanines, loop size and the nature of the central monovalent cations affect G-quadruplex conformation. Solution of high resolution deoxyribonucleic acid (DNA; refer to list of abbreviations in appendix) G-quadruplex crystal structures by NMR and X-ray crystallography highlights their structural diversity.[1,3,4,8–15] Both intermolecular and intramolecular oligonucleotide arrangements can assemble into G-quadruplexes. Intermolecular quadruplexes consist of either two or four guanine-rich strands that assemble together with the guanine bases pointing inside the quadruplex. In contrast, intramolecular quadruplexes are unimolecular structures that form when tandem guanine repeats separated by a few non-guanine nucleotides fold to form guanine rings held together by Hoogsteen-hydrogen bonds. G-quadruplexes can be further classified as parallel, antiparallel or mixed. G-quadruplexes are designated as parallel if all strands involved in the formation of the stacked G-tetrads have the same polarity and antiparallel if they run in opposite directions.

Figure 1. Schematic representation of a G-quadruplex. A. Hoogsteen-hydrogen bonding between four guanines assembled in a ring. A monovalent cation positioned in the central ion channel coordinates with O_6 carbonyl groups. B. A diagram of an intramolecular G-quadruplex. Successive G-tetrads stack on top of each other. Figure by G-quadruplex.jpg: Julian Huppert Jlh29 derivative work: Iridos (G-quadruplex.jpg) [CC-BY-SA-2.5 (http://creativecommons.org/licenses/by-sa/2.5)], via Wikimedia Commons.

A.

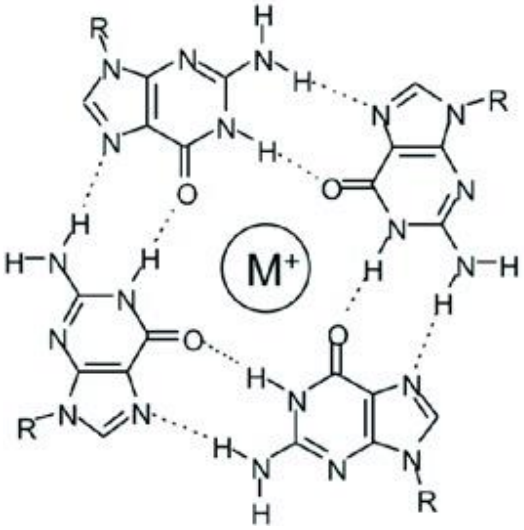

B.

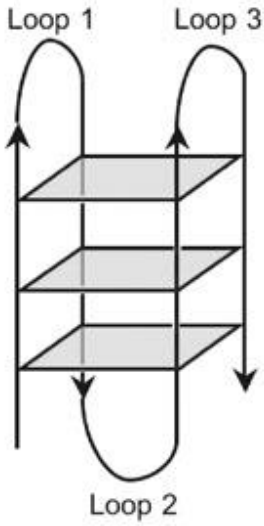

Despite their conformational variability, G-quadruplexes possess high thermodynamic stability due to stacking of the G-tetrads. The crystal structure of a parallel intramolecular quadruplex formed by a 22 nucleotide sequence from human telomeric DNA ($d[AGGG(TTAGGG)_3]$) in the presence of potassium cations shows guanine glycosidic bonds in the *anti*-conformation and π-π stacking interactions between the three planar G-tetrads.[3] Propeller-like loops connect the bottom of one strand with the top of another without blocking the terminal G-tetrads.[3] Potassium cations are positioned centrally between the G-tetrad planes in a bi-pyramidal arrangement with the eight O_6 carbonyl groups.[3] The same sequence folds into an antiparallel quadruplex in the presence of sodium cations.[3] Of the studied sequences, most assume a parallel arrangement in the presence of potassium and antiparallel arrangement in the presence of sodium cations, although high resolution structures of tetramolecular parallel quadruplexes in the presence of sodium cations although exist.[1–3] Since the cytoplasmic concentration of potassium in much higher than the concentration of sodium in a cellular environment, it is likely that G-quadruplex structures produced in the presence of potassium are more physiologically relevant.[16] In contrast to DNA quadruplexes, less ribonucleic acid (RNA) G-quadruplex structures are available. A crystal structure of TERRA RNA quadruplex, a recently discovered non-coding transcript of telomeric DNA, in the presence of potassium shows two parallel three-layer quadruplexes held together by stacking interactions between terminal G-tetrads.[17] The structure of RNA G-quadruplex appears to be affected by the ribonucleotide 2'-hydroxyl group that contributes to hydrogen bonding within the quadruplex and determines the preference for a parallel conformation.[17]

1.2 DISTRIBUTION OF G-QUADRUPLEX MOTIFS WITHIN HUMAN GENOME

Until recently, G-quadruplexes were assumed to be aberrant secondary structures formed by G-rich nucleotides *in vitro*. However, within the last few years both DNA and RNA G-quadruplexes were visualized inside human cells and quadruplex forming motifs have been implicated in telomere maintenance, genome expression through translational and transcriptional regulation, immunoglobulin switching, epigenetic instability and disease.[18–20] *In situ* analysis of the human genome predicted 376 000 potential G-quadruplex forming motifs.[21] In order to eliminate random G-rich sequences from the results, the algorithm used in this analysis took into account loop length between guanine runs suitable for G-quadruplex formation. G-quadruplex forming motifs are overrepresented in proto-oncogenes and parts of the genome associated with transcriptional control, growth factors, cell growth, cell signalling and development as well as in 5'-untraslated regions (UTRs), first intron and 3'-UTRs regions of mRNA transcripts.[22] They are underrepresented in regions of the genome associated with cell adhesion, ubiquitin cycle, nucleosome assembly, G-protein coupled receptors and tumor suppressor genes.[22] G-quadruplexes have also been implicated in epigenetic control of gene expression. Hyper-methylated CG sequences associated with transcriptional silencing are underrepresented within regions of the genome predicted to fold into G-quadruplexes.[23]

G-quadruplex forming motifs were predicted in over 40% of human gene promoters.[24] Both c-*MYC* and c-*KIT* oncogenes are transcriptionally repressed by G-quadruplex structures within their respective promoter regions.[6,25] Expression of c-*MYC* is associated with cellular proliferation, breast, colon and cervical cancers as well as myeloid leukemias. The c-*KIT* oncogene encodes a tyrosine receptor and is associated with stem cell growth and differentiation.[6] Human proto-oncogene *NRAS* and human zinc finger protein Zic-1 are

transcriptionally supressed by quadruplexes located in the 5'-UTRs of their respective mRNAs.[26,27] In addition to acting as *cis*-regulatory elements for transcription and translation, G-quadruplexes also regulate mRNA splicing. In *vitro* stabilization of a quadruplex structure within intron 6 of mRNA of the human telomerase reverse transcriptase (hTERT), an enzyme responsible for telomere extension in germ cells, results in production of an inactive splice variant of the enzyme.[28] Splicing of tumor suppressor gene p53 mRNA is also regulated by a G-quadruplex in its intron 3.[29] A shorter splice variant produces a protein that regulates p53 activity. Polymorphisms at the G-quadruplex forming sequence in the *TP53* gene, which codes for p53 protein, correlate with early-onset cancers. Moreover, a G-quadruplex motif within the internal ribosome entry site (IRES) on the 5'-alternatively translated region (ATR) of mRNA for human fibroblast factor FGF-2 is required for 5'-cap independent translation of FGF-2.[30]

G-quadruplexes are also found within telomeres. In humans, 3' terminal chromosomal regions consist of several kilobasepairs of TTAGGG sequence repeats followed by a single stranded tail a few hundred base pairs in length, which is required for loading of hTERT.[31] Telomeres protect linear DNA from degradation during replication.[31] DNA polymerase, which copies single-stranded DNA in the 5' to 3' direction, uses an RNA primer to load onto the strand and initiate replication. The leading strand is copied continuously, but the lagging strand is copied in short fragments called Okazaki fragments and the spaces vacated by the RNA primers are later filled by DNA ligase to produce a continuous DNA strand. However, the terminal 5' sequence is lost during each replication event because DNA ligase can only fill and ligate regions bordered by DNA on each side. Thus, telomeres protect the coding regions of chromosomes from shortening with each replication event. Hence, telomeres determine the number of replications that a somatic cell can undergo before apoptosis.[32] In addition, telomeres

are thought to protect chromosomal ends from fusion with each other.[31] Telomeres exist in complex with proteins thought to be involved in hTERT recruitment and protection of single-stranded ends.[20] Numerous G-quadruplexes structures separated by flexible linkers form on telomeric strands and their arrangement has been described as "beads-on-a-string".[33]

G-quadruplexes have been detected inside human cells using a G-quadruplex-specific single chain antibody called BG4.[18] Only about one quarter of the detected spots were located at telomeres, confirming *in situ* studies of G-quadruplex distribution within the genome.[18] In addition, the lowest number of quadruplexes was detected during the G0/G1 stage of the cell cycle, when no DNA replication occurs and about a five-fold increase in signal was detected during the S phase, when DNA replicates, suggesting that quadruplexes form in G-rich sequences when single-stranded DNA is exposed.[18] In contrast to regulatory quadruplexes, these non-specific secondary structures may cause the DNA and RNA polymerases to stall, effectively inhibiting replication or transcription and leading to disease.[34] Interestingly, however, the stalling by DNA polymerase δ was found to persist *in vitro* even after the G-quadruplex forming sequences were mutated to disrupt quadruplex formation.[35] Nevertheless, polymorphisms resulting in expansion of G-rich repeats are associated with syndromes characterized by increased chromosomal abnormalities, double-stranded DNA breakages and premature termination of transcription.[36–40] Neurodegenerative disorders amyotrophic lateral sclerosis (ALS) and frontotemporal dementia (FTD) are associated with expansion of GGGGCG repeats in intron 1 of the *C9orf72* gene.[40] While healthy individuals carry less than 30 repeats of this sequence, a fraction of affected patients have between 700 and 1600 repeats.[41] Using circular dichroism and nuclear magnetic resonance, this expansion has been shown to form parallel G-quadruplex *in vitro*.[40] Increased number of the GGGGCG repeat within the *C9orf72* is correlated

with accumulation of aborted mRNA transcripts of the *C9orf72* gene, which causes nucleolar stress and cytotoxicity.[40] Aborted transcripts might sequester proteins important for ribosomal assembly or regulation, making them unavailable to other transcripts or some transcripts may be translated into dysfunctional or misfiled proteins that later aggregate in the cytoplasm.[40] Thus, specialized helicases capable of unwinding G-quadruplexes are required for normal genome function.

1.3 G-QUADRUPLEX HELICASES

Bloom syndrome protein (BLM), Werner protein (WRN) and Faconi anemia group J protein (FANCJ) are a few of the DNA helicases shown to be able to unwind DNA G-quadruplex structures into single-stranded DNA.[36–38,42] Deficiency in the BLM protein that unravels G-quadruplex DNA in the 3' to 5' direction is associated with Bloom's syndrome, which is characterized by increased incidence of chromatid breaks and sister chromatid exchange leading to growth retardation, impaired fertility, immunodeficiency and cancers.[36] The WRN helicase unwinds bimolecular G-quadruplexes formed by sequence $d(CGG)_7$ in the 3' to 5' direction and exhibits 3' to 5' exonuclease activity.[37] Unlike BLM and WRN, FANCJ, another DNA G-quadruplex helicase, unwinds the quadruplex in the 5' to 3' direction and its deficiency is associated with increased number of deletions within G-rich regions of DNA.[38,42] Interaction between BLM and FANCJ has been detected, suggesting that they might simultaneously unravel quadruplexes from opposite ends.[34]

Numerous compounds specific for G-quadruplexes have been identified[3,20,43] Acridines, tetra-N-pyridyl porphyrins and triazine derivatives bind G-quadruplexes.[3] Additionally, a dye *N*-methyl mesoporphyrin IX (NMM) is specific for parallel quadruplexes.[11] The crystal structure of

a human telomeric quadruplex bound by NMM reveals π-π stacking between the terminal G-tetrad of the quadruplex and the compound.[11] Unlike in the antiparallel quadruplex, the loops of the parallel quadruplex do not block the terminal G-tetrad faces, allowing them to participate in stacking interactions with ligands. The N-methyl group of NMM was found to fit inside the quadruplex ion channel and interact with the potassium cation.[11] Another compound, carboxyPDS, is specific for RNA quadruplexes and together with BG4 antibody has been used to visualize RNA G-quadruplexes in the cytoplasm of human cells.[19]

1.4 RNA HELICASE ASSOCIATED WITH *AU*-RICH ELEMENT IS A MAJOR G-QUADRUPLEX RESOLVASE

RNA Helicase Associated with *AU*-rich element (RHAU) (also known as DHX36 and DNA resolvase 1) is a prominent G-quadruplex resolvase in human cells. RHAU is a DEAH-box helicase composed of 1008 amino acids, weighs 119 kDa and is encoded by the *Dhx36* gene. Two splice variants of RHAU were detected in HeLa cell extracts.[44] The full length RHAU mainly localizes in the nucleus and RHAU$^{\Delta 14}$, which lacks a 14 amino acid long nuclear localization signal, is only present in the cytoplasm.[44] The concentration of RHAU was found to be significantly higher in the nucleus than in the cytoplasm.[44] Originally, RHAU was identified as a protein involved in mRNA deadenylation and decay for its ability to co-precipitate with ARE^{uPA}-mRNA from HeLa cell extracts.[44] It was also found to interact with the exosome and polyadenylate-specific ribonucleases (PARN) in an RNA-independent fashion and with NFAR1 and HuR in a RNA-mediated fashion.[44] Since its discovery, RHAU has been implicated in mRNA destabilization, transcriptional and translational regulation and blood cell formation.[44–47] RHAU was detected in nucleoplasm and also in nuclear speckles in HeLa cells and was found to

associate with RHA helicases p68 and p72 within nucleolar caps upon transcriptional arrest.[48] Nuclear speckles are areas of the nucleus enriched in pre-mRNA splicing factors and nucleolar caps contain mostly RNA binding proteins that aggregate in the nucleolus during periods of cellular stress or arrested transcription. RHAU also binds and targets RNA to stress granules, which are cytoplasmic structures that sequester cellular proteins and RNA during periods of stress to the cell.[49] RHAU functions as a transcriptional inducer for TNAP, which is involved in bone formation and differentiation.[45] Moreover, RHAU is involved in translational regulation of transcriptional regulator Yin Yang 1 (YY1) and a homeobox transcription factor PITX1 that has been implicated in development and cancer.[46,50] RHAU was shown to be essential for murine hematopoiesis and its depletion in developing mouse embryos resulted in hemolytic anemia and blood cell differentiation defects.[47] RHAU was also co-precipitated with neuronal precursor-micro-RNA-134 (miRNA134) and was implicated in miRNA134-dependent gene inhibition and control of growth of dendritic spines, which are dendritic membranous protrusions that receive signals from axons as synaptic junctions.[51]

RHAU has sustained most attention as a G-quadruplex resolvase. RHAU was found to unwind tetramolecular G-quadruplexes *in vitro*, but was later shown to display higher affinity for tetramolecular RNA quadruplexes.[52,53] In a subsequent study, RHAU's ability to unwind intramolecular G-quadruplexes in an ATP-dependent fashion was shown to out-compete its tetramolecular G-quadruplex resolving activity *in vitro*.[54] RHAU binds and resolves the RNA G-quadruplex in the 5' terminal region of the RNA component of the human telomerase reverse transcriptase enzyme, allowing proper formation of the P1 helix structure required for correct incorporation of nucleotides into the template used for reverse transcription of telomeric DNA.[55–57] Human telomerase reverse transcriptase is a ribonucleoprotein active in highly proliferating

germ and cancer cells, but not in somatic cells. It is composed of a catalytic protein subunit (TERT) and a human telomerase reverse transcriptase RNA component (hTR) that acts as a template for telomeric extension. Activation of hTERT in somatic cells is associated with unchecked replication and cancerous tumors. Sexton *et al*. and Giri *et al*. separately showed that RHAU binds and unwinds a 5' terminal quadruplex in hTR *in vitro*[54,56]. These findings were confirmed by Lattmann *et al*., who demonstrated that RHAU targets hTERT *in vivo*.[55]

Human telomerase RNA is 452 nucleotides long and is transcribed by RNA polymerase II. Eight highly conserved regions (CRs) numbered from 5' to 3' have been identified in vertebrate telomerase RNA. [58] Ten conserved helical structures called paired helices (P) make up four domains in the secondary structure of vertebrate telomerase RNA. The conserved domains include the pseudoknot domain, the CR4-CR5 domain, the BOX H/ACA domain and the CR7 domain. CR4-CR5 is required for hTERT binding to hTR and formation of an active hTERT holoenzyme. CR1, located 45 nucleotides downstream of the 5' end of hTR, encodes the template sequence 5'-CUAACCCU-3' required for extension of telomeric DNA. In humans, incorporation of correct nucleotides into the template sequence during reverse transcription is accomplished by constraining the sequence through hTR-hTERT interaction and RNA-RNA base-pairing upstream of the sequence.[59] Helix P1 that forms upstream of the 5' region of the template acts as an anchor that tethers the template region through a short linker. Disruption of P1 helix formation through mutation results in synthesis of telomeric repeats of incorrect length and incorporation of extra nucleotides into the template.[59] The P1 helix consists of two regions, P1a and P1b, separated by a loop. The P1b structure is essential for correct template incorporation. The 5' terminal region of hTR can form several quadruplexes that might incorporate the nucleotides required to form the P1 helix. Nucleotides 1 to 17 correspond to the

minimal length of hTR capable of G-quadruplex formation *in vitro*.[57] These quadruplexes may serve to protect the single stranded 5' terminus of hTR from degradation during maturation of hTERT, but they must be unwound to allow P1 helix formation and correct template demarcation.[56,57] Bisquinolinium compounds Phen-DC_3 and Phen-DC_6 and a 2,6-pyridine-dicarboxamide derivative 360A are G-quadruplex-specific ligands that have been shown to prevent P1 helix formation in hTR by binding to and stabilizing the 5'-terminal G-quadruplex structures in hTR.[60,61] These compounds had an inhibitory effect on P1 helix formation only if the oligonucleotide sequence was able to form G-quadruplex and the effect was absent if the sequence was mutated to disrupt G-quadruplex formation.[61] Since the RHAU binds and unwinds both DNA and RNA synthetic G-quadruplexes formed by the 5' terminus of hTR and knockdown of endogenous RHAU in HEK293T cells results in observed reduction in average telomere length.[57] Additionally, deletion studies have revealed that RHAU-specific motif (RSM) within the N-terminus of RHAU is required for quadruplex recognition (Figure 2).[56] The RSM region of RHAU is conserved among vertebrates, suggesting its evolutionary importance and RHAU's physiological significance.[56] The helicase domain is not required for quadruplex binding, which is independent of ATP-hydrolysis.[56]

Figure 2. Schematic representation of the putative domains of the full-length RHAU protein. The domains were predicted using homology structure modeling conducted using the SWISS-MODEL server accessed throught the ExPASy web server (Accession Number Q9H2U1).[62–65]

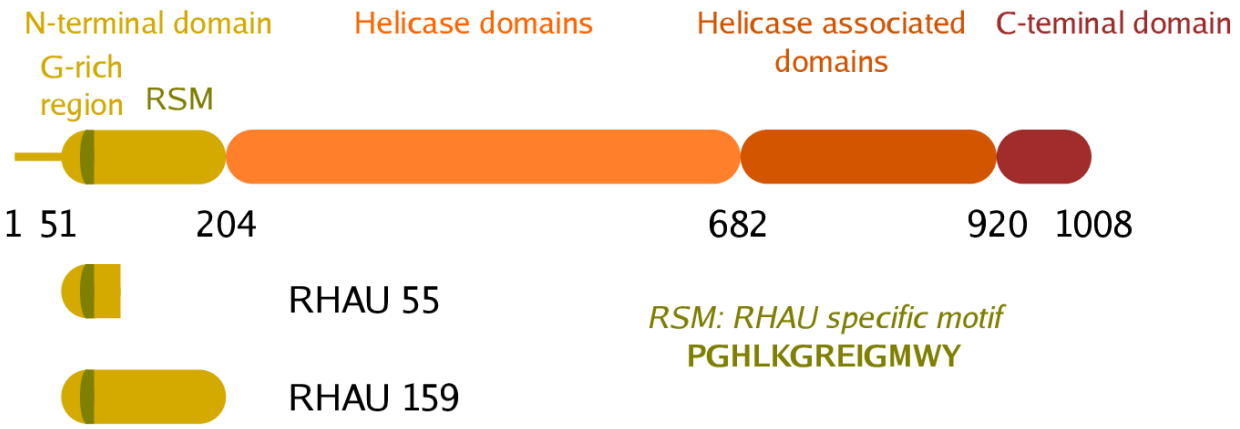

RHAU is classified as a RNA helicase belonging to the DEAH family. DHA and RNA helicases are multifunctional ATP-dependent enzymes involved in nucleic acid remodelling and nucleoprotein dissociation. Most helicases belong to the phylogenetically conserved superfamily 2 (SF2), which is subdivided into five families based on conserved structure and sequence. Most of the helicases studied belong to the DEAD and DExH/DEAH families that share conserved structural elements.[66–71] SF2 helicases share seven conserved motifs encompassed within two domains that fold into a claw-like structure with an ATP-binding and hydrolysis site in the cleft between the two domains. The DEAD (Asp-Glu-Ala-Asp) and DExH/DEAH (Asp-Glu-x-His/Asp-Glu-Ala-His) families are classified based on the amino acids in the ATP-binding site. Additional N-terminal and C-terminal domains have protein-specific functions. Both DEAD-box and DExH/DEAH-box helicases unwind duplex DNA in the 3’ to 5’ direction, but unlike non-processive DEAD-box helicases that unwind only small helices, DExH/DEAH-box helicases translocate along the nucleotide strand and unwind helices up to several dozen base pairs in

length.[67] In addition to local structural rearrangement, helicases can remodel protein-RNA and protein-DNA complexes by displacing bound proteins. The high resolution structure of the yeast RNA helicase Prp43p, which shares considerable sequence similarity with RHAU, has become available recently and provides some insight into the mode of action of RNA helicases.[68] Prp43p lacks an extended N-terminal domain present in RHAU, but the structure suggests that a conformational change induced by ATP hydrolysis is required to uncover the RNA binding site.[68] The N-terminal domain of RHAU is followed by a flexible linker that may be involved in the conformational rearrangement of the protein required to deliver the bound quadruplex to the helicase domain. RHAU is an important helicase to be studied in the context of its interaction with G-quadruplexes.

1.5 OBJECTIVES

Here, we investigated the binding of the N-terminal construct of RHAU (residues 53-105) with DNA analog of the quadruplex-forming nucleotides 1-20 from the human telomerase RNA component. We used an integrated biophysical approach including circular dichroism, dynamic light scattering and small angle X-ray scattering to study the interaction between $RHAU_{53\text{-}105}$ and $hTR_{1\text{-}20}$ DNA. In addition, several potential conditions for crystallization of the complex between $RHAU_{53\text{-}105}$ and $hTR_{1\text{-}20}$ DNA_{c2} were identified. Although structures of complexes between G-quadruplexes and small molecule ligands are available, there is a lack of information regarding the recognition of G-quadruplexes by helicases. This is an important path for investigation due to widespread involvement of G-quadruplexes in DNA and RNA metabolism and in the correct functioning of hTERT in particular.

2. Materials and Methods

2.1 G-QUADRUPLEX PREPARATION

Synthetic hTR_{1-20} DNA sequence 5'-GGGUUGCGGAGGGUGGGCCU-3' was purchased from Alpha DNA, Canada and was dissolved in 20 mM HEPES, pH 7.5, 100 mM KCl at a concentration of 10 mM. The solution was heated to 95° C and was allowed to passively cool to room temperature in a water bath. The solution was stirred continuously. The folded quadruplex was purified using the HiLoad Superdex 75 26/60 size exclusion chromatography (SEC) column and was eluted in 20 mM HEPES, pH 7.5, 100 mM KCl buffer. The quadruplex eluted in two peaks. The first peak to elute was identified at hTR_{1-20} DNA_{C1} and the second as hTR_{1-20} DNA_{C2}. The extinction coefficient ($\varepsilon_{260\ nm}$=189 000 $M^{-1}cm^{-1}$) used to calculate hTR_{1-20} DNA concentration was calculated using IDT SciTools® (Primer-Quest Program, Integrated DNA Technologies).

2.2 EXPRESSION AND PURIFICATION of $RHAU_{53-105}$

$RHAU_{53-105}$ was expressed and purified according to the protocol described previously.[57] The gene coding for $RHAU_{53-105}$ with an N-terminal hexahistidine (His_6) tag followed by a thrombin cleavage site was cloned into a pET15b vector carrying an ampicillin resistance gene. $RHAU_{53-105}$ was expressed in *Escherichia coli* (*E. coli*) strain BL2(DE3) in luria broth (LB) in the presence of ampicillin. A 25 ml pre-culture grown overnight was used to start a 1.8 L culture grown at 37 °C with constant shaking at 200 rpm. Expression was induced with addition of Isopropyl β-D-1-thiogalactopyranoside (IPTG) to final concentration of 5 mM once OD_{600} reached 0.6. Cells were grown for three hours and the pellet was collected by centrifugation at

6000 rpm for 20 minutes at 4 °C. The pellet was frozen at -80 °C. The cells were thawed on ice and lysed in 20 mM sodium phosphate, 2 mM imidazole, 6 M guanidine hydrochloride, pH 7.0 in the presence of proteases using homogenization followed by sonication. The protein was purified by affinity chromatography using Talon® cobalt resin. The column was equilibrated using two column volumes of 20 mM sodium phosphate, 2 mM imidazole, pH 7.0 followed by two volumes of the lysing buffer. Following the loading of the cell lysate, the column was washed using the equilibration buffer and the protein was refolded and eluted in 150 mM imidazole, pH 7.0, I=300 mM (NaCl). The purified protein was concentrated to 1 mg/ml and dialysed overnight into 10 mM HEPES, pH 7.5, I=154 mM (NaCl). Thrombin was added to the dialysis membrane to cleave the His_6 tag. Following dialysis and His_6 tag cleavage, thrombin was removed using a HiTrap benzamidine FF column (GE Healthcare). The extinction coefficient ($\varepsilon_{280\ nm}$=6990 $M^{-1}cm^{-1}$) for $RHAU_{53-105}$ was calculated using the ExPASy ProtParam and the concentration of the protein was determined spectrophotometrically.[72]

2.3 EXPRESSION AND PURIFICATION of $RHAU_{53-150}$

Originally, expression and purification of $RHAU_{53-209}$ was attempted by a fellow laboratory member. His_6-tagged $RHAU_{53-209}$ was cloned into the pET15b vector and expressed in *E. coli* strain BL21(DE3) cells using the same protocol as for $RHAU_{53-105}$. Purification and His_6 tag cleavage were also carried out as described for $RHAU_{53-105}$. The molecular weight of the resulting protein, estimated using SDS-PAGE, was less than expected for $RHAU_{53-209}$, suggesting that the protein degraded during purification. Mass spectrometric analysis revealed the resulting protein was $RHAU_{53-150}$.

2.4 PREPARATION OF PROTEIN-QUADRUPLEX COMPLEXES

$RHAU_{53-105}$ and hTR_{1-20} DNA were mixed in 1:1 molar ratio and diluted in 20 mM HEPES, pH 7.5, 100 mM KCl. Each component was added at a concentration of 10 mM. The solution was left at room temperature for 20 minutes and was then concentrated to 5 mg/ml. The concentration of the complex was measured spectrophotometrically and calculated using the absorption coefficient for the DNA component. The complexes were purified on a Superdex 200 10/300 GL SEC column and eluted using 20 mM HEPES, pH 7.5, 100 mM KCl. The extinction coefficient for the nucleotide component ($\varepsilon_{260\ nm}$=189 000 $M^{-1}cm^{-1}$) was used to calculate the concentration of the complexes.

2.5 UV-VISIBLE ABSORPTION SPECTROSCOPY

Spectra were obtained on the Evolution 260 Bio spectrophotometer (Thermo Scientific) using a temperature controlled 1.0 mm sample cell and 1.0 mm water-filled reference cell. Sample and buffer were each measured in triplicate and the average buffer spectrum was subtracted from the average sample spectrum. The percentage of hypochromicity at 297 nm was calculated by dividing the difference between ε_{297} for folded DNA and ε_{297} for unfolded DNA by ε_{297} for unfolded DNA.

2.6 ELECTROPHORETIC MOBILITY SHIFT ASSAY

$RHAU_{53-105}$ and either hTR_{1-20} DNA_{c1} or hTR_{1-20} DNA_{c2} were mixed in molar ratios ranging from 0:1 to 6:1 in 20 mM HEPES, pH 7.5, 100 mM KCl, 20% glycerol and 140 mM glycine. Final nucleic acid concentration was 200 nM in each solution. The samples were well-mixed, centrifuged at 13 000 rpm for 45 seconds and loaded onto 12% polyacrylamide TBE gels.

The gels were resolved by electrophoresis at 75V and 4°C for 2.5 hours. The gels were stained for 10 minutes using either SYBR Green II or N-methylmesoporphyrin IX and imaged using the FluorChem Q imaging system (Cell Biosciences).

2.7 CIRCULAR DICHROISM SPECTROPOLARIMETRY

Spectra were collected on the J-810 spectropolarimeter (Jasco Inc.) calibrated using (2.583 mM (1*S*)-(+)-camphor-10-sulfonic acid monohydrate; Alfa Aesar). 1.0 mm cell and integration times of 8 seconds were used for 350 to 220 nm, 1.0 mm cell and integration time of 32 seconds for 220 to 200 nm and 0.1 mm cell and integration time of 32 seconds for 200 to 180 nm. Sample concentration was 30 to 50 µM in the 1.0 mm cell and 200 µM in 0.1 mm cell. Sample and buffer were measured separately in triplicate and the average buffer spectrum was subtracted from the average sample spectrum. Nucleic acids were measured in 20 mM HEPES, pH 7.5, 100 mM KCl or in 20 mM sodium phosphate, pH 7.5, 100 mM KF. $RHAU_{53\text{-}105}$ was measured in 10 mM HEPES, pH 7.5, I =154 mM (NaCl). Nucleic acid spectra were normalized by number of bases per unit volume and protein spectra were normalized by number of peptide bonds per unit volume. Melting curves for nucleic acids were obtained by recording ellipticity at 263 nm over a range of temperatures in 20 mM HEPES, pH 7.5, 100 mM KCl. The protein-quadruplex complexes were measured in 20 mM HEPES, pH 7.5, I=100 mM KCl and the spectra were normalized by number of nucleotide bases per unit volume.

2.8 DYNAMIC LIGHT SCATTERING

Data were collected using the Nano-S Dynamic Light Scattering system (Malvern Instruments Ltd., Malvern, UK) equipped with a 633 nm laser and using a 173° scattering angle.

All solutions were filtered using a 0.1 μm centrifugal filter (Millipore, USA) and allowed to equilibrate to 20°C for 20 minutes prior to data collection. Samples and buffer were measured separately in a 45 μL quartz cuvette at a range of concentrations. RHAU was measured in 10 mM HEPES, pH 7.5, I=154 mM and nucleic acids and quadruplexes in 20 mM HEPES, pH 7.5, 100 mM KCl. Measurements were collected in automatic mode and four measurements were obtained for each concentration.

2.9 SMALL ANGLE X-RAY SCATTERING

Data collection and data analysis were performed by Dr. Trushar Patel. Data was collected with a Rigaku 3-pinhole camera (S-MAX3000) on a 200-mm multi-wire 2D detector calibrated with gold particles (NIST, Standard Reference Material 8012, National Institute of Standards and Technology, Maryland, USA). The instrument was equipped with a Rigaku MicroMax+200 microfocus sealed tube and Confocal Max-Flux (CMF) optics. Cu-Kα radiation at 1.54 Å was generated and used to illuminate the sample. Buffer and sample at a range of concentrations were each exposed for 2 to 4 hours and the raw data was reduced using Rigaku's SAXGUI data processing software. The momentum transfer, s, was defined as follows: $s=4\pi\sin\theta/\lambda$, where θ is the scattering angle and λ is the wavelength. Individual data sets were merged and radius of gyration (R_g) and maximum particle dimension (D_{max}) were calculated using the GNOM program.[73] Ab initio modelling were carried out using the experimentally determined R_g and D_{max} parameters. Multiple low resolution solution conformations were generated by DAMMIN, a program that relies on temperature-dependent simulated annealing.[74] Goodness of fit parameter (χ) was calculated for each model to assess its quality and passing models were averaged using the DAMAVER program.[75] HYDROPRO was used to calculate the

hydrodynamic parameters for the models.[76] Following SAXS data collection, DLS measurements were carried out for each sample to check whether degradation occurred due to radiation exposure.

2.10 CRYSTALLIZATION TRIALS

In an effort to identify suitable conditions for crystallization of $hTR_{1-20}DNA_{c1}$, $hTR_{1-20}DNA_{c2}$, $hTR_{1-20}DNA_{c1}{\cdot}RHAU_{53-105}$ and $hTR_{1-20}DNA_{c2}{\cdot}RHAU_{53-105}$, crystallization trials were conducted using commercial crystallization kits from Hampton Research (CA, USA). The quadruplexes and complexes were prepared as described in the preceding sections of this report. Crystallization conditions were tested using the vapour diffusion method. Sitting drops composed of 1 µL of the species to be crystallized and 1 µL of reservoir solution were set-up in 96-well plates. Each well contained 50 µL of reservoir solution. All species were filtered using 0.2 µm filters prior to crystallization. The plates were covered with clear protective film and incubated at 20 °C. Crystal Screen HT and Natrix HT screening kits (Hampton Research, CA, USA) were used to test crystallization conditions for of $hTR_{1-20}DNA_{c1}$ at 7.26 mg/ml and $hTR_{1-20}DNA_{c2}$ at 5.41 mg/ml. Crystal Screen HT, PEG/ION HT, Index HT and Natrix HT screening kits (Hampton Research, CA, USA) were utilized to test possible crystallization conditions for $hTR_{1-20}DNA_{c1}{\cdot}RHAU_{53-105}$ and $hTR_{1-20}DNA_{c2}{\cdot}RHAU_{53-105}$. The complex of $RHAU_{53-105}$ with $hTR_{1-20}DNA_{c1}$ was tested at 5.09 mg/ml and 8.65 mg/ml and the complex with $hTR_{1-20}DNA_{c2}$ was tested at 5.41 mg/ml. The concentrations of the complexes refer to the concentration of $RHAU_{53-105}$ in the complex only. Concentration of the oligonucleotide component was determined spectrophotometrically and then the concentration of protein was calculated on the basis of equimolar binding between $hTR_{1-20}DNA$ and $RHAU_{53-105}$.

To optimize the crystallization conditions for $RHAU_{53-105}$·hTR_{1-20} DNA_{c2} identified using the initial PEG/ION HT screen, forty-eight conditions were tested using the vapour diffusion method (Table 1). Hanging drops composed of 2 µL of the complex at 5.5 mg/ml (protein component) and 2 µl of the crystallization solution were set up in 24-well plates. Each well contained 1.00 ml of reservoir solution. The plates were incubated at 20 °C.

In addition, hTR_{1-20} DNA_{c2}·$RHAU_{53-105}$ was further screened using Crystal Screen 1 and Crystal Screen 2 (Hampton Research, CA, USA). Hanging drops composed of 2 µL of complex containing 4.00 mg/ml of $RHAU_{53-105}$ and 2 µL of reservoir solution were prepared on slides and suspended above wells containing 1.00 ml of reservoir solution. The wells were sealed with grease and the plates were incubated at 20 °C. The crystal plates were observed daily for the first week, every three days for the next week, weekly for the subsequent month and monthly for the remainder of the time.

Table 1. Crystallization solutions screened in an effort to optimize crystals of $RHAU_{53\text{-}105}{\cdot}hTR_{1\text{-}20}DNA_{c2}$ initially obtained in 0.2 M formate salt, 20 % w/v PEG 3500.

Plate 1	1	2	3	4	5	6
A	PEG 3350 18% w/v $CHKO_2$ 0.2 M	PEG 3350 19% w/v $CHKO_2$ 0.2 M	PEG 3350 20% w/v $CHKO_2$ 0.2 M	PEG 3350 21% w/v $CHKO_2$ 0.2 M	PEG 3350 22% w/v $CHKO_2$ 0.2 M	PEG 3350 23% w/v $CHKO_2$ 0.2 M
B	PEG 3350 18% w/v $CHKO_2$ 0.2 M KCl 0.1 M	PEG 3350 19% w/v $CHKO_2$ 0.2 M KCl 0.1 M	PEG 3350 20% w/v $CHKO_2$ 0.2 M KCl 0.1 M	PEG 3350 21% w/v $CHKO_2$ 0.2 M KCl 0.1 M	PEG 3350 22% w/v $CHKO_2$ 0.2 M KCl 0.1 M	PEG 3350 23% w/v $CHKO_2$ 0.2 M KCl 0.1 M
C	PEG 3350 18% w/v HCOONa 0.2 M	PEG 3350 19% w/v HCOONa 0.2 M	PEG 3350 20% w/v HCOONa 0.2 M	PEG 3350 21% w/v HCOONa 0.2 M	PEG 3350 22% w/v HCOONa 0.2 M	PEG 3350 23% w/v HCOONa 0.2 M
D	PEG 3350 18% w/v HCOONa 0.2 M KCl 0.1 M	PEG 3350 19% w/v HCOONa 0.2 M KCl 0.1 M	PEG 3350 20% w/v HCOONa 0.2 M KCl 0.1 M	PEG 3350 21% w/v HCOONa 0.2 M KCl 0.1 M	PEG 3350 22% w/v HCOONa 0.2 M KCl 0.1 M	PEG 3350 23% w/v HCOONa 0.2 M KCl 0.1 M
Plate 2	**1**	**2**	**3**	**4**	**5**	**6**
A	PEG 3350 18% w/v NH_4HCO_2 0.2 M	PEG 3350 19% w/v NH_4HCO_2 0.2 M	PEG 3350 20% w/v NH_4HCO_2 0.2 M	PEG 3350 21% w/v NH_4HCO_2 0.2 M	PEG 3350 22% w/v NH_4HCO_2 0.2 M	PEG 3350 23% w/v NH_4HCO_2 0.2 M
B	PEG 3350 18% w/v NH_4HCO_2 0.2 M KCl 0.1 M	PEG 3350 19% w/v NH_4HCO_2 0.2 M KCl 0.1 M	PEG 3350 20% w/v NH_4HCO_2 0.2 M KCl 0.1 M	PEG 3350 21% w/v NH_4HCO_2 0.2 M KCl 0.1 M	PEG 3350 22% w/v NH_4HCO_2 0.2 M KCl 0.1 M	PEG 3350 23% w/v NH_4HCO_2 0.2 M KCl 0.1 M
C	PEG 3350 18% w/v $Mg(HCO_2)_2$ 0.2 M KCl 0.1 M	PEG 3350 19% w/v $Mg(HCO_2)_2$ 0.2 M KCl 0.1 M	PEG 3350 20% w/v $Mg(HCO_2)_2$ 0.2 M KCl 0.1 M	PEG 3350 21% w/v $Mg(HCO_2)_2$ 0.2 M KCl 0.1 M	PEG 3350 22% w/v $Mg(HCO_2)_2$ 0.2 M KCl 0.1 M	PEG 3350 23% w/v $Mg(HCO_2)_2$ 0.2 M KCl 0.1 M
D	PEG 3350 18% w/v $CHKO_2$ 0.2 M	PEG 3350 19% w/v $CHKO_2$ 0.2 M	PEG 3350 20% w/v $CHKO_2$ 0.2 M	PEG 3350 21% w/v $CHKO_2$ 0.2 M	PEG 3350 22% w/v $CHKO_2$ 0.2 M	PEG 3350 23% w/v $CHKO_2$ 0.2 M

2.11 TEST FOR EXPRESSION OF $RHAU_{53-1008}$ IN *ESCHERICHIA COLI (E. coli)*

Expression of His_6-tagged $RHAU_{53-1008}$ in pET-15b plasmid was attempted in *E. coli* strain BL21(DE3) cells. A pre-culture containing 50 ml of LB media and 100 µg/ml ampicillin was inoculated and grown overnight at 37 °C with constant shaking at 200 rpm. In the morning, 1.5 ml of the pre-culture was used to inoculate another 50 ml of LB with ampicillin. The newly inoculated culture was incubated at 37 °C with constant shaking at 200 rpm until OD_{600} reached 0.6, at which time expression was induced with addition of IPTG at 5 mM final concentration. The culture was incubated for two additional hours under the same conditions and sampled every half hour. The collected samples were then denatured by addition of 10% (w/v) sodium dodecyl sulfate and Laemmli buffer in a 1:1 ratio and heating at 95 °C for 4 minutes prior to analysis by SDS-PAGE.

Since expression of His_6-$RHAU_{53-1008}$ in *E. coli* strain BL21(DE3) proved unsuccessful, expression was carried out in *E. coli* strain BL21(DE3) supplemented with the RIPL plasmid. *E.coli* strain BL21(DE3)-RIPL cells were transformed with His_6-$RHAU_{53-1008}$ in pET-15b plasmid by electroporation. The protocol described for expression of $RHAU_{53-105}$ in *E. coli* strain BL21(DE3) cells was followed to express His_6-$RHAU_{53-1008}$ in *E. coli* BL21(DE3) RIPL cells. Following expression, the cells were collected by centrifugation and frozen at -80 °C.

2.12 PURIFUCATION OF His_6-$RHAU_{53-1008}$

Purification of His_6-$RHAU_{53-1008}$ was attempted by affinity chromatography using Ni-NTA agarose beads (Qiagen, USA). The frozen pellet was lysed in 40 ml of 20 mM Tris/Tris-HCl, pH 8.5, I=150 mM (NaCl). Serine protease inhibitors were added to the pellet to prevent protein degradation. The cells were lysed by homogenization followed by sonication. The

supernatant was separated from the pellet by centrifugation at 22 000 g for 30 minutes at 4 °C. Prior to addition of the lysate supernatant, the Ni-NTA agarose beads were washed with three volumes of 20 mM Tris/Tris-HCl, pH 8.5, I=150 mM (NaCl). The beads were pelleted by centrifugation at low speed for 2 minutes, the buffer was discarded, the lysate supernatant was added and the beads were incubated with the lysate supernatant for 1.5 hours. Then, the beads were pelleted and washed with two volumes of 20 mM Tris/Tris-HCl, pH 8.5, I=150 mM (NaCl) followed by two volumes of 20 mM HEPES, pH = 7.5, I=150 mM (NaCl). Elution of the His_6-tagged protein was attempted using an imidazole gradient. The beads were successively washed with two volumes of 20 mM imidazole/imidazole HCl, pH 6.0, I=150 mM (NaCl), one volume of 250 mM imidazole/imidazole HCl, pH 6.0, I=150 mM (NaCl) and three volumes of 500 mM imidazole/imidazole HCl, pH 6.0, I=150 mM (NaCl). The beads were further washed and stored in 20% ethanol. The entire purification procedure was performed at 4 °C.

2.13 WESTERN BLOT FOR DETECTION OF $RHAU_{53-1008}$

To check the success of purification of His_6-$RHAU_{53-1008}$ by affinity chromatography, a western blot was performed using a mouse anti-RHAU antibody. A sample of the cell lysate as well as the samples of washing buffers collected during attempted purification of His_6-$RHAU_{53-1008}$ were denatured and resolved by SDS-PAGE. A pre-stained molecular size ladder was loaded on the gel. The proteins were then transferred from the polyacrylamide gel to a nitrocellulose membrane soaked in 10 mM CAPS, pH 11.0, 10 % v/v methanol using semi-dry electroblotting at 0.11 A for 45 minutes. Following the transfer of the proteins to the nitrocellulose membrane, the membrane was blocked using Phosphate Buffered Saline with Tween 20 (PBS-T) with 5 % (w/v) Coffee Whitener (No Name Brand). After one hour incubation at room temperature, the

membrane was washed with PBS-T buffer for three consecutive 10 minute intervals. The membrane was then incubated for one hour with mouse anti-RHAU antibody in blocking solution, washed with PBS-T buffer and incubated for addition 1 hour with horseradish peroxidase (HRP) conjugated anti-mouse antibody in blocking solution. The membrane was again washed with PBS-T, incubated in Luminata Forte Western HRP substrate (EMD Millipore, USA) for 4 minutes at room temperature and imaged using a fluorescent detector.

2.14 CLONING OF $RHAU_{53\text{-}1008}^{\Delta 14}$.pCEP-Pu.BM40

To obtain $RHAU_{53\text{-}1008}^{\Delta 14}$.pCEP-Pu.BM40, $RHAU_{1\text{-}52}$ was first deleted in $RHAU_{1\text{-}1008}^{\Delta 14}$ in pcDNA3 by in-vitro site-directed mutagenesis. $RHAU_{53\text{-}1008}^{\Delta 14}$.pcDNA3 was copied and amplified from $RHAU_{1\text{-}1008}^{\Delta 14}$.pcDNA3 using the polymerase chain reaction (PCR). The PCR reaction was performed using the Phusion High-Fidelity DNA Polymerase enzyme (Thermo-Scientific), which produces products with blunt ends. The following primers were used: 5'-CATCCCGGGCACCTGAAAGGCCGCGAAATCGGCATGTGG-3' (forward) and 5'-AAGCTTGGGTCTCCCTATAGTGAGTCGTATTAATTTC-3'. The final reaction mixture contained the following components: 1X Phusion HF buffer (supplied by Thermo-Scientific), 0.1 mM each dNTP, 0.5 µM forward primer, 0.5 µM reverse primer, 100 ng template, 3% (v/v) dimethyl sulfoxide (DMSO) and 1 U of Phusion High-Fidelity DNA Polymerase. The components were mixed on ice and the PCR reaction was carried out in the S1000™ Thermal Cycler (BIO-RAD) using a three-step protocol. Initial denaturation lasted 3 minutes at 98 °C. Then, 32 cycles were completed under the following conditions: 15 sec denaturation at 98 °C, 30 sec annealing at 65 °C, 4 minutes and 15 seconds extension at 72 °C. The final extension step took place at 72 °C for 5 minutes. After completion of the PCR reaction, the PCR mixture was

loaded into a 0.8% agarose gel and resolved by gel electrophoresis. The plasmid corresponding to $RHAU_{53\text{-}1008}^{\Delta 14}$.pcDNA3 was extracted from the gel using the GeneJET Gel Extraction Kit (Thermo-Scientific). The purified linear plasmid was circularized and ligated using T4 DNA Ligase (Thermo-Scientific). The ligation mixture was purified using the GeneJET PCR Purification Kit (Thermo-Scientific).

Then, $RHAU_{53\text{-}1008}^{\Delta 14}$ was copied and amplified from $RHAU_{53\text{-}1008}^{\Delta 14}$.pcDNA3 by PCR. The forward primer 5'-AGCCCCGCTAGCTCATCATCACCACCATCATGACGATGACGATAAGCATCCCGGGCACCTGAAAGGCCGCGAA -3' contains a NheI restriction site followed by a His_6 tag and an enterokinase cleavage site. The reverse primer 5'-GCCGCCCTCGAGTCAGCTGTAATATCCATCCTGGAATCGTGGCGG-3' contains an XhoI restriction site. The PCR reaction contained the following components: 1X Phusion HF buffer (supplied by Thermo-Scientific), 0.1 mM each dNTP, 0.5 µM forward primer, 0.5 µM reverse primer, 100 ng template and 1 U of Phusion High-Fidelity DNA Polymerase. The reaction was performed the S1000^{TM} Thermal Cycler (BIO-RAD) under the following conditions: initial denaturation for 3 minutes at 98 °C, 32 cycles of 15 second denaturation at 98 °C, 30 second annealing at 65 °C and 2 minute extension at 72 °C, followed by a final 5 minute extension at 72 °C. After completion of the PCR reaction, the PCR mixture resolved by gel electrophoresis on a 0.8% agarose gel. The band corresponding to $RHAU_{53\text{-}1008}^{\Delta 14}$ was extracted from the gel using the GeneJET Gel Extraction Kit (Thermo-Scientific) and digested with NheI and XhoI restriction enzymes, which produce sticky ends upon DNA cleavage. The pCEP-Pu.BM40 vector was also digested with NheI and XhoI. Both $RHAU_{53\text{-}1008}^{\Delta 14}$ and pCEP-Pu.BM40 vector were purified using the GeneJET PCR Purification Kit (Thermo-Scientific) after completion of the digestion

reactions, concentration of each species was measured spectrophotometrically and the two oligonucleotide segments were ligated using T4 DNA Ligase (Thermo-Scientific). The ligation mixture was incubated at room temperature for 15 minutes and used to transform z-competent *E. coli* strain DH5α cells. The transformed cells were grown on LB and ampicillin agar at 37 °C for 24 hours, individual colonies were sampled and grown in LB and ampicillin cultures overnight at 37 ° and the cells were lysed and plasmid extracted using the GeneJET Plasmid Extraction Kit (Thermo-Scientific). The size and sequence of the obtained plasmid was confirmed by gel electrophoresis and sequencing. All sequencing reactions were carried out by a commercial facility.

3. Results

3.1 DNA ANALOG OF THE hTR_{1-20} SEQUENCE ASSUMES G-QUADRUPLEX SECONDARY STRUCTURE IN SOLUTION

In an effort to analyze the binding interaction between the RSM of RHAU and G-quadruplex oligonucleotides, synthetic DNA of the hTR_{1-20} sequence was used. The DNA quadruplex was prepared in the presence of 100 mM KCl and purified on a preparative size exclusion column. hTR_{1-20} DNA eluted as two peaks, suggesting that the two species differ in their conformations since they have identical molecular weights. Conformation 1, which eluted prior to conformation 2, comprised about two-thirds of the sample. To determine whether conformations 1 and 2 of the hTR_{1-20} DNA quadruplex could interconvert, conformation 1 fractions collected during the first purification run were heated at 95 °C for ten minutes, allowed to passively cool to room temperature and purified on the preparative HiLoad Superdex 75 26/60 column (GE Healthcare). This procedure was repeated four times. The elution profiles for each of the four runs (Figure 3A) indicate that upon heating, a portion of hTR_{1-20} DNA_{c1} interconverts to hTR_{1-20} DNA_{c2}, although the proportion of hTR_{1-20} DNA_{c2} decreases with each subsequent heating-cooling cycle (Figure 3B).

The interconversion between hTR_{1-20} DNA_{c1} and hTR_{1-20} DNA_{c2} was further assessed using UV-Vis spectrophotometry. Figure 4A shows UV-Vis spectra collected for hTR_{1-20} DNA at 20 °C, at 80 °C and at 20 °C following cooling to room temperature after heating at 80 °C. An increase in absorbance at 260 nm at 80 °C relative to 20 °C is indicative of G-quadruplex unfolding. Following the heating to 80 °C and cooling back to 20 °C, the sample produced a spectrum that is intermediate between the spectra obtained at 20 °C and at 80 °C.

The interconversion between hTR_{1-20} DNA_{c2} and hTR_{1-20} DNA_{c1} was also investigated by UV-Vis spectrophotometry. In contrast to hTR_{1-20} DNA_{c1}, hTR_{1-20} DNA_{c2} produces identical UV-Vis spectra at 20 °C before and after heating at 80 °C, suggesting that the heating-cooling cycle did not induce a conformational change in the sample. Moreover, circular dichroism spectra for hTR_{1-20} DNA_{c2} were not affected by heating of the sample to 80 °C and cooling back to room temperature (Figure 4B). Neither UV-Vis spectrophotometry nor spectropolarimetry show evidence of conversion of hTR_{1-20} DNA_{c2} to hTR_{1-20} DNA_{c1}.

The purified hTR_{1-20} DNA was further analyzed on a Superdex 200 SEC column and conformation 1 eluted ahead of conformation 2 (Figure 5). Both conformations stained with SYBER Green II as well as with the quadruplex specific dye N-methylmesoporphyrin IX (Figure 6). In contrast, the hTR_{1-43} RNA sequence that was mutated to prevent quadruplex formation did not stain with N-methylmesoporphyrin IX. UV-Vis measurements for hTR_{1-20} DNA_{c1} and hTR_{1-20} DNA_{c2} shown in Figure 7 indicate hyperchromicity at 260 nm and hypochromicity at 297 nm at 80°C in comparison to 20°C. The extinction coefficients at 297 nm for hTR_{1-20} DNA_{c1} and hTR_{1-20} DNA_{c2} decreased by 30.9% and 37.5%, respectively, at 80°C relative to 20°C. UV CD spectra for both conformations of hTR_{1-20} DNA confirm the presence of quadruplex secondary structure (Figure 8). Both hTR_{1-20} DNA_{c1} and hTR_{1-20} DNA_{c2} were analyzed by spectropolarimetry in 20 mM HEPES, pH 7.5, 100 mM KCl and 20 mM sodium phosphate, pH 7.5, 100 mM KF. Due to substitution of HEPES and KCl with sodium phosphate and KF, it was possible to extend collection of circular dichroism data to lower wavelengths. The spectra in both buffers for each conformation of the quadruplex are comparable, except the lower wavelength maximum is shifted left (Figure 8). Both spectra show a maximum at 263 nm and a minimum at 242 nm. In addition, a second maximum is observed at 207 nm for hTR_{1-20} DNA_{c1} and at 209 nm

for $hTR_{1\text{-}20}$ DNA_{c2}. The two spectra also differ in the region between 280 and 315 nm, where conformation 1 produced a sloping shoulder that is absent for conformation 2. Peak dampening, indicative of the loss of the quadruplex structure was observed at 80°C for both conformations (Figure 9). Using the ellipticity measured at 263 nm, the melting temperature was estimated to be 70°C for $hTR_{1\text{-}20}$ DNA_{c1} and 64°C for $hTR_{1\text{-}20}$ DNA_{c2}.The recorded melting curves are displayed in Figure 10.

SAXS experiments were performed to obtain low resolution structural information about $hTR_{1\text{-}20}$ DNA quadruplexes in solution. DLS measurements that were conducted prior to SAXS data collection reveal the presence of monodisperse species in solution (Figure 11). Each quadruplex conformation was analyzed by SAXS at multiple concentrations. The resulting data sets were merged to produce a scattering profile for each quadruplex species (Figure 12A). Pair distribution functions (*P(r)*), which describe the distances between all observed electron pairs in a molecule, were constructed using the scattering information. Bell-shaped *P(r)* functions were obtained for each quadruplex and were used to extract the radii of hydration (r_G) and maximum distances of the molecules (D_{max}) (Figure 12B). The hydrodynamic parameters for the two conformations are similar. All hydrodynamic parameters are summarized in Table 1. Numerous low resolution models were calculated for each quadruplex and were later merged to produce an average surface envelope for each conformation. Each conformation of the quadruplex appears as a disk-like structure with two concave faces (Figure 12C). The normalized spatial discrepancy (NSD) values, ≤ 0.51 for both conformations of the quadruplex, indicate similarity between individually calculated models. In addition, χ values (0.8 for $hTR_{1\text{-}20}$ DNA_{c1} and 0.9 for $hTR_{1\text{-}20}$ DNA_{c2}) suggest excellent agreement between experimentally obtained and model-based

hydrodynamic parameters. DLS measurements obtained after SAXS data collections showed absence of detectable degradation following exposure to radiation.

Figure 3. Purification of hTR_{1-20} DNA by size exclusion chromatography. A. Elution profiles for hTR_{1-20} DNA purified on a HiLoad Superdex 75 26/60 column (GE Healthcare). Following each run, the fractions corresponding to conformation 1 (peak on the left) were collected, heated at 95 °C for 10 minutes, cooled to room temperature and purified on the same column. This procedure was repeated four times. B. A bar graph showing the reduction in the amount of interconversion of hTR_{1-20} DNA_{c1} to hTR_{1-20} DNA_{c2} with each heating-cooling cycle.

A

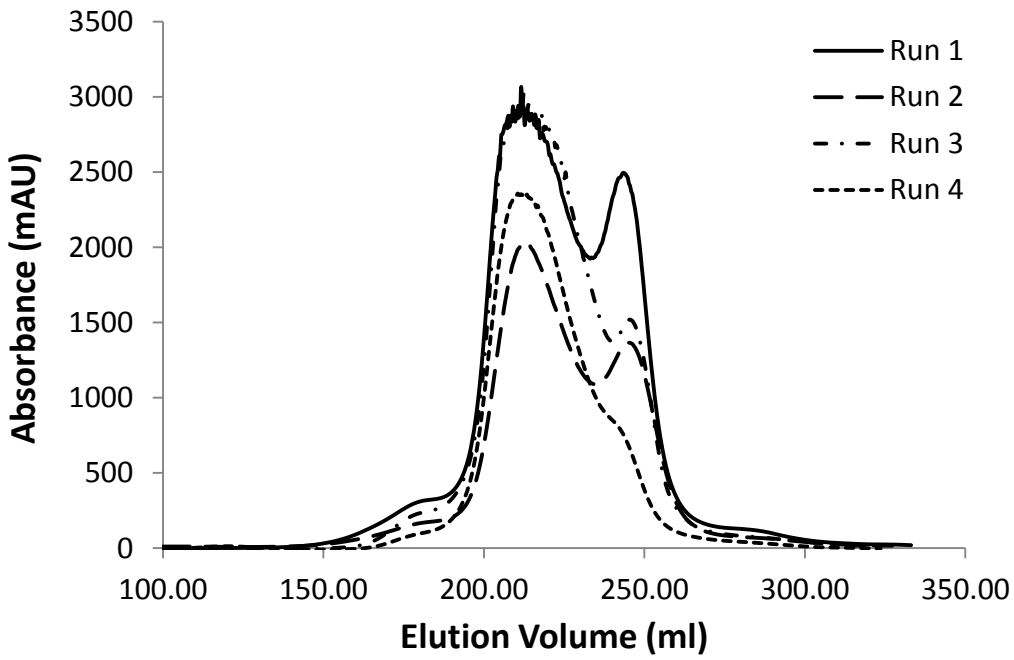

B

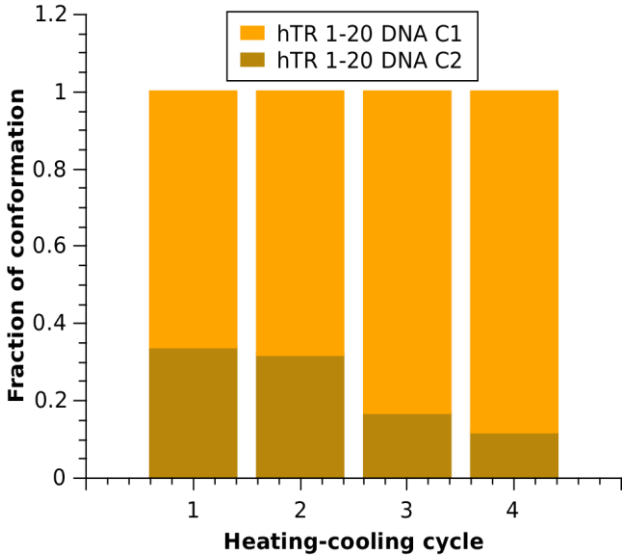

Figure 4. The analysis of interconversion between the two conformations of hTR_{1-20} DNA by UV-Vis spectrophotometry and spectropolarimetry. UV-Vis spectra for hTR_{1-20} DNA_{c1} (A) and hTR_{1-20} DNA_{c2} (B) measured at 20 °C (*solid line*), 80 °C (*dashed line*) and 20 °C after sample was heated at 80 °C and passively cooled (*dotted line*). C. CD spectrum measured for hTR_{1-20} DNA_{c2} at 20°C before (*solid line*) and after (*dotted line*) heating at 80 °C.

A

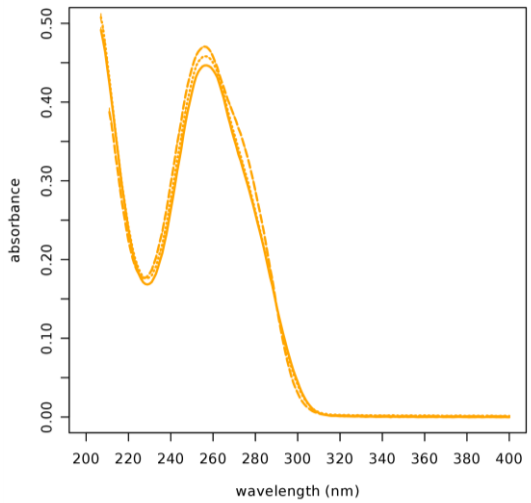

B

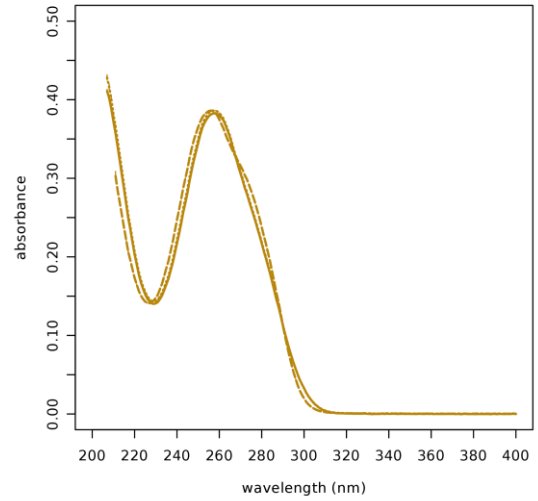

C

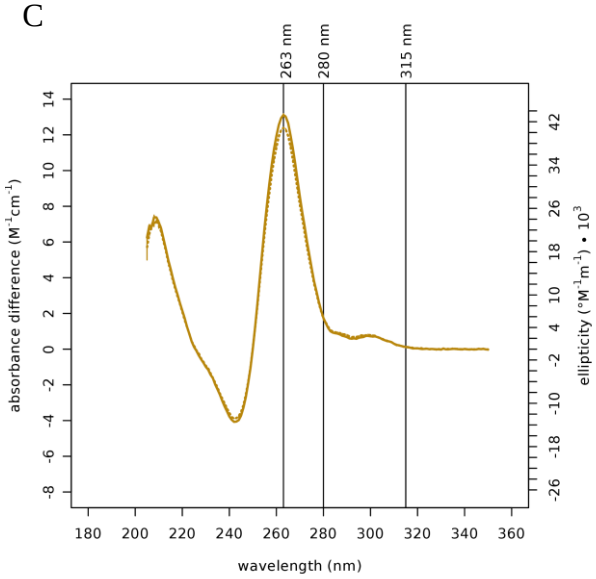

Figure 5. Elution profiles of N-terminal RHAU, hTR_{1-20} G-quadruplexes and their complexes acquired from the Superdex 200 10/300 GL size exclusion chromatography column. The following colour scheme was used: $RHAU_{53-105}$, *red, solid*; hT_{1-20} DNA_{c1}, *orange, solid*; hTR_{1-20} DNA_{c2}, *goldenrod, solid*; $RHAU_{53-105}$·hTR_{1-20} DNA_{c1}, *orange, dotted*; hTR_{1-20} DNA_{c2}, *goldenrod, dotted*. All species except $RHAU_{53-105}$ were eluted in 20 mM HEPES, pH 7.5, I=100 mM KCl. $RHAU_{53-105}$ was eluted in 10 mM HEPES, pH 7.5, I=154 mM (NaCl).

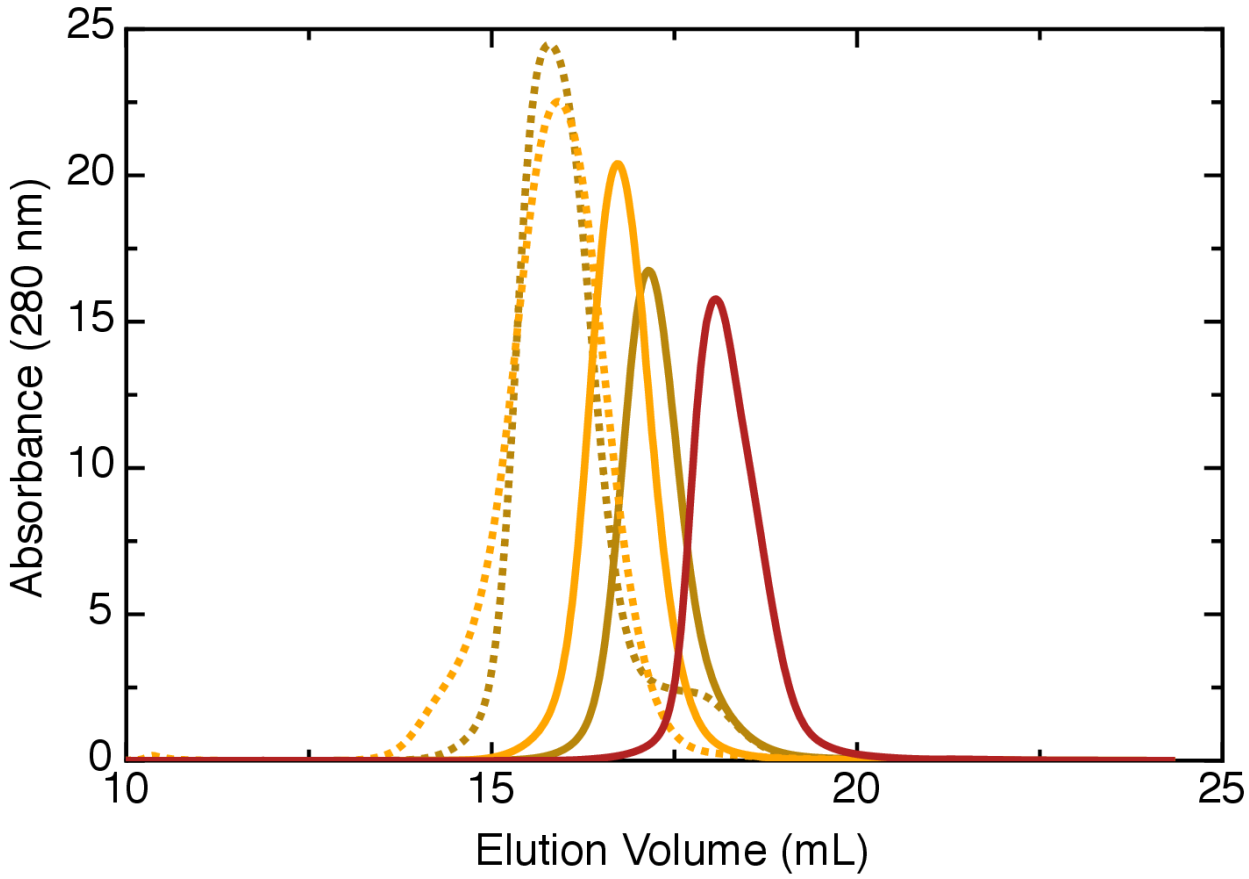

Figure 6. Electrophoretic Mobility Shift Assay with $RHAU_{53-105}$ and hTR_{1-20} DNA quadruplex. A. $RHAU_{53-105}$ shifts hTR_{1-20} DNA_{c1} under native conditions. The hTR_{1-20} DNA_{c1} stains with both SYBR Green II (*left*) and N-methylmesoporphyrin IX (*right*). The hTR_{1-43} RNA mutated to prevent quadruplex formation only stains with SYBR Green II. B. $RHAU_{53-105}$ shifts hTR_{1-20} DNA_{c2} under native conditions. The hTR_{1-20} DNA_{c1} stains with both SYBR Green II (*left*) and N-methylmesoporphyrin IX (*right*). The hTR_{1-43} RNA mutated to prevent quadruplex formation only stains with SYBR Green II.

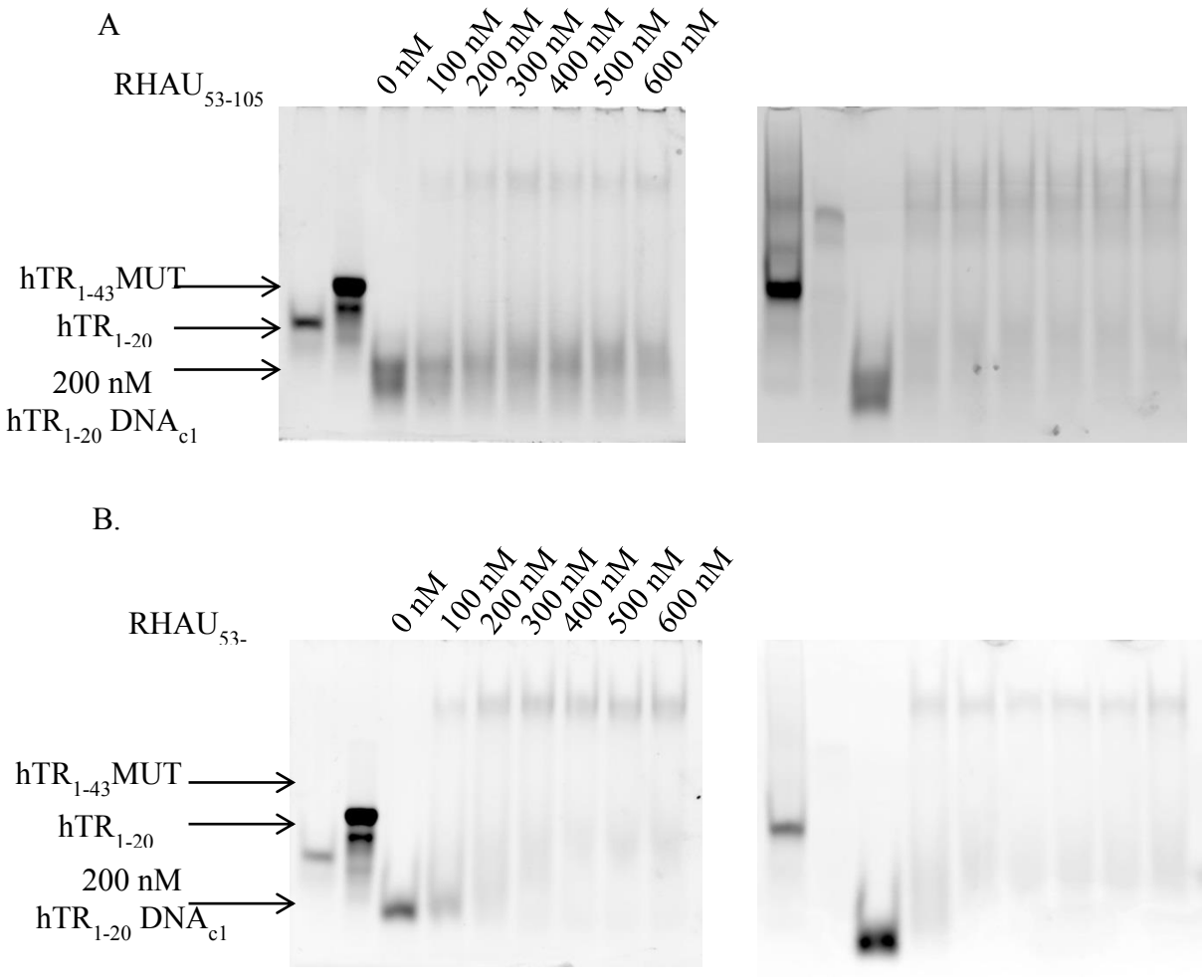

Figure 7. Indication of G-quadruplex structure in UV-visible spectra obtained for hTR_{1-20} DNA_{c1} (*orange*) and hTR_{1-20} DNA_{c2} (*goldenrod*). The spectra were recorded at 20 °C (*solid*) and 80 °C in 20 mM HEPES, pH 7.5, I=100 mM KCl. Hypochromicity of 30.9% for hTR_{1-20} DNA_{c1} and 37.5% for hTR_{1-20} DNA_{c2} is evident at 297 nm (Inset). Slight hyperchromicity is seen at 260 nm for both quadruplexes.

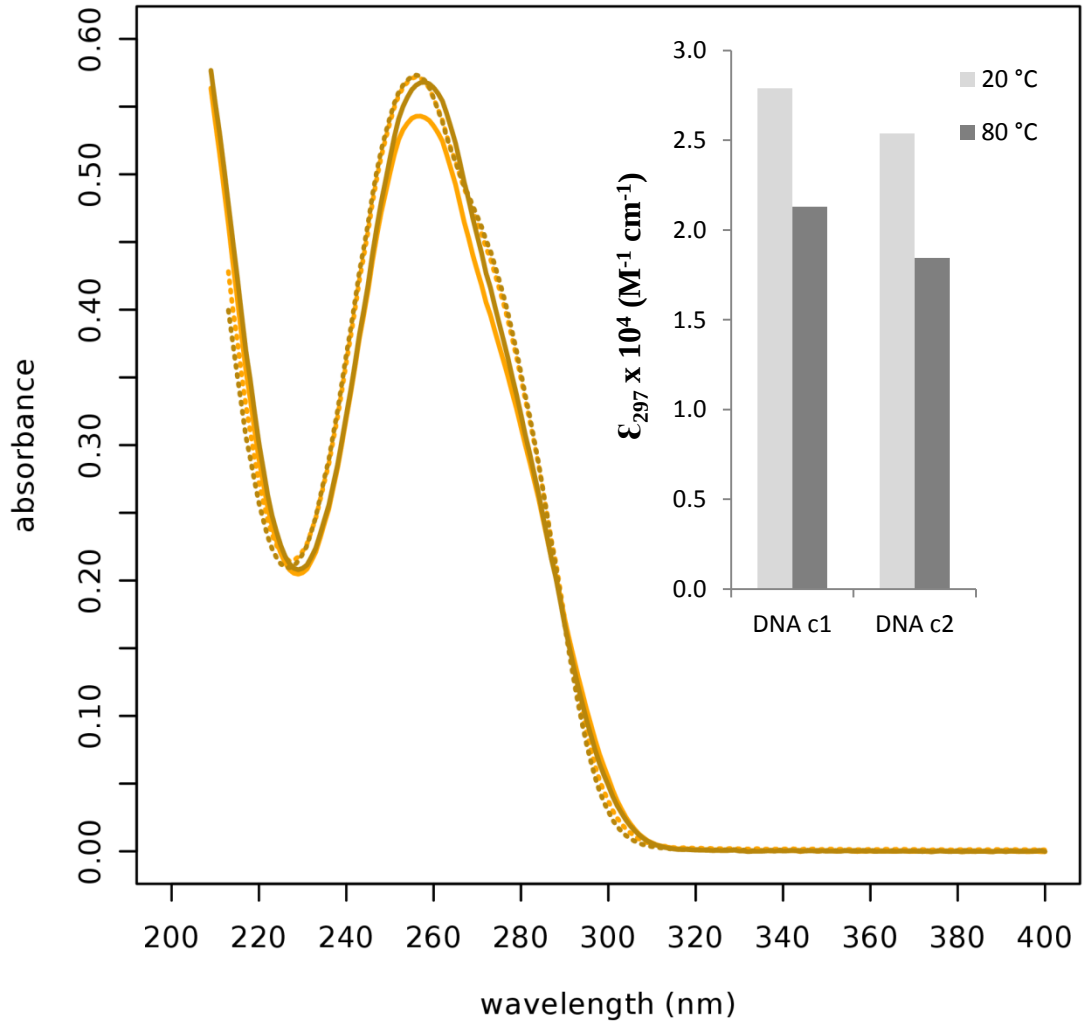

Figure 8. Effect of buffer composition on the conformations of $hTR_{1\text{-}20}$ DNA_{c1} (*orange*) and $hTR_{1\text{-}20}$ DNA_{c2} (*goldenrod*). Circular dichroism spectra for each conformation of $hTR_{1\text{-}20}$ DNA in 20 mM HEPES, pH 7.5, 100 mM KCl (*solid line*) and 20 mM sodium phosphate, pH 7.5, 100 mM KF (*dashed line*) are compared.

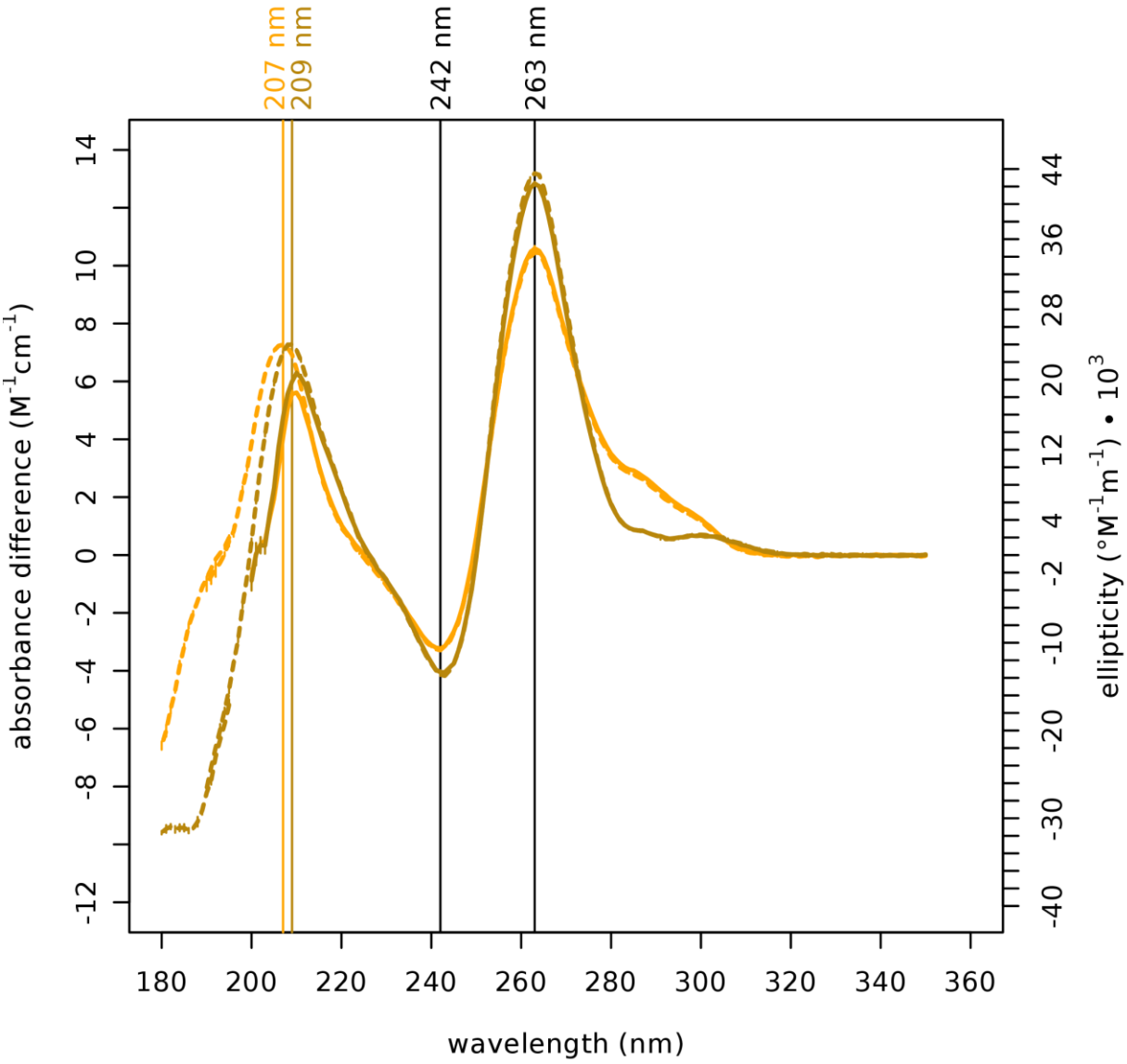

Figure 9. Analysis of hTR_{1-20} DNA G-quadruplexes by spectropolarimetry. Far-UV CD spectra of hTR_{1-20} DNA_{c1} (*orange*) and hTR_{1-20} DNA_{c2} (*goldenrod*) and 20 °C (solid) and 80 °C (only standard deviations of three measurements are shown). Vertical error bars show standard deviations. All spectra were recorded in 20 mM HEPES, pH 7.5, I=100 mM KCl. Maxima and minima of the spectra are indicated by vertical lines.

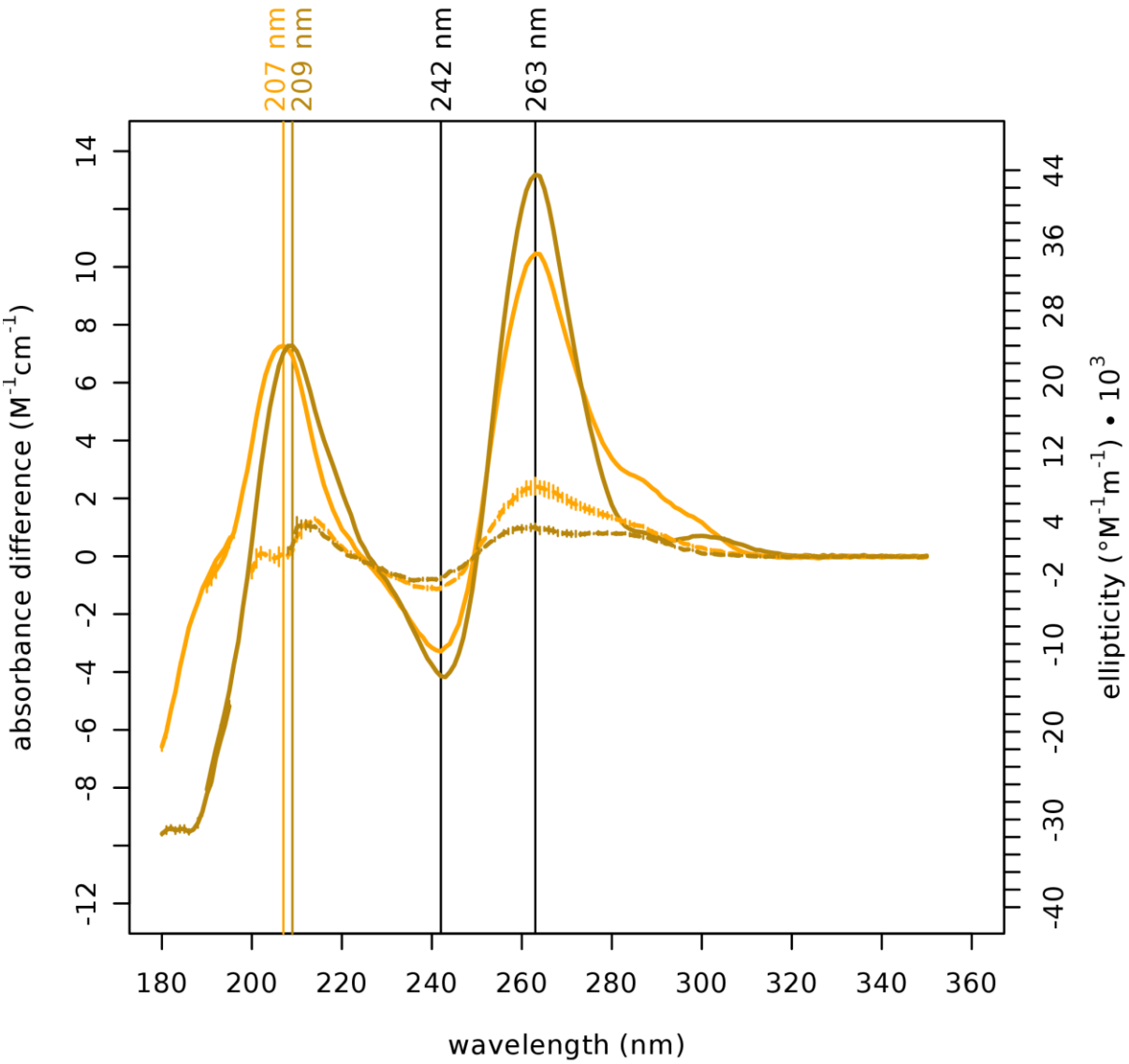

Figure 10. Melting curves of the G-quadruplexes obtained by spectropolarimetry at 263 nm. The midpoints of transition indicated by vertical lines were estimated at ~70 °C for $hTR_{1\text{-}20}$ DNA_{c1} (*orange*) and at ~64 °C for $hTR_{1\text{-}20}$ DNA_{c2} (*goldenrod*).

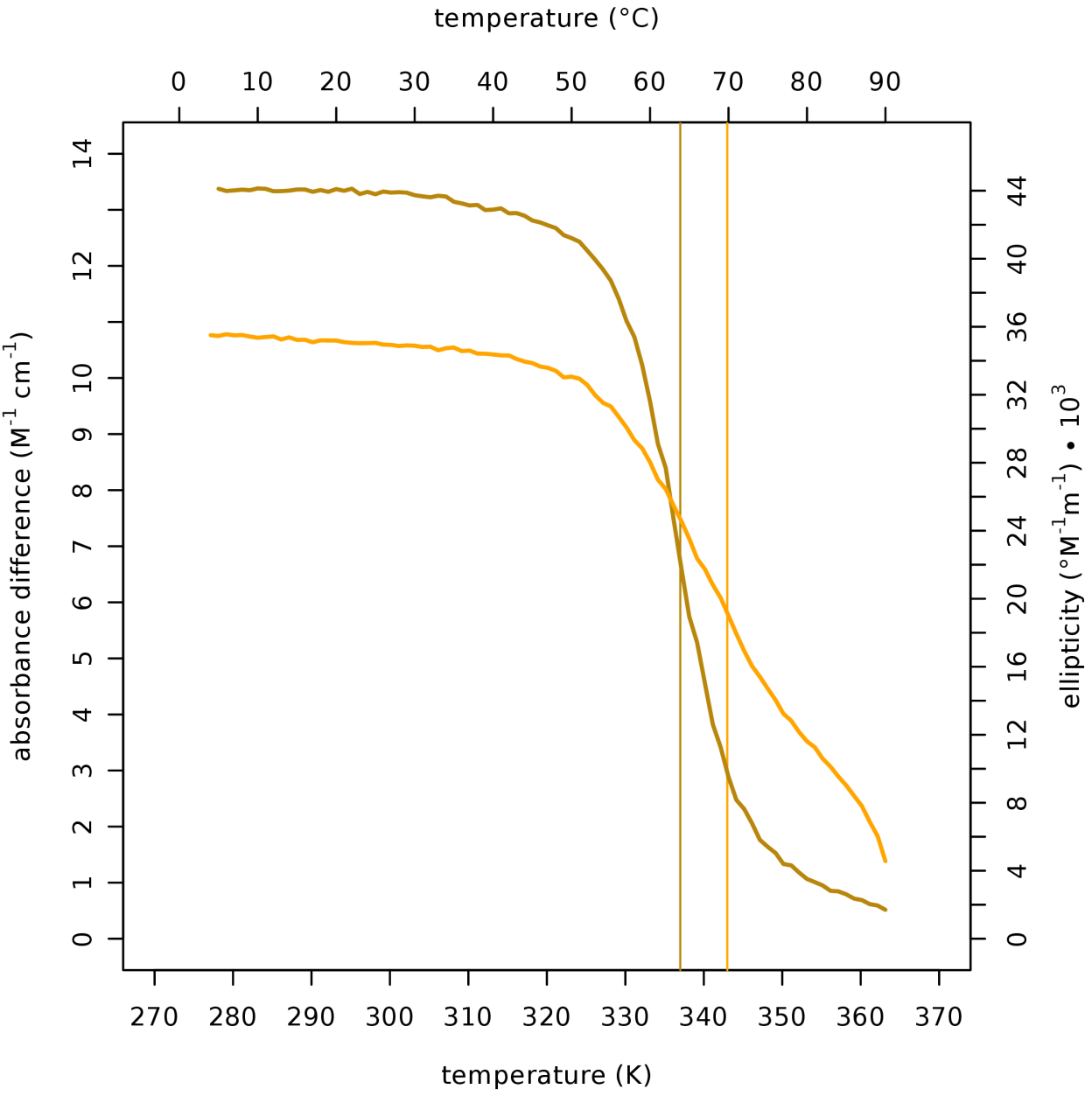

Figure 11. Dynamic light scattering profiles of N-terminal RHAU constructs, quadruplexes and their complexes. The concentration (*Conc.*) dependence of the r_H of $RHAU_{53\text{-}105}$ is shown in the inset. The following colour scheme was used: $RHAU_{53\text{-}105}$, *red, solid*; $RHAU_{53\text{-}150}$, black, solid; $hT_{1\text{-}20}$ DNA_{c1}, *orange, solid*; $hTR_{1\text{-}20}$ DNA_{c2}, *goldenrod, solid*; $RHAU_{53\text{-}105}$·$hTR_{1\text{-}20}$ DNA_{c1}, *orange, dotted*; $hTR_{1\text{-}20}$ DNA_{c2}, *goldenrod, dotted*. All species except $RHAU_{53\text{-}105}$ and $RHAU_{53\text{-}150}$ were analyzed in 20 mM HEPES, pH 7.5, I=100 mM KCl. $RHAU_{53\text{-}105}$ and $RHAU_{53\text{-}150}$ were analyzed in 10 mM HEPES, pH 7.5, I=154 mM (NaCl).

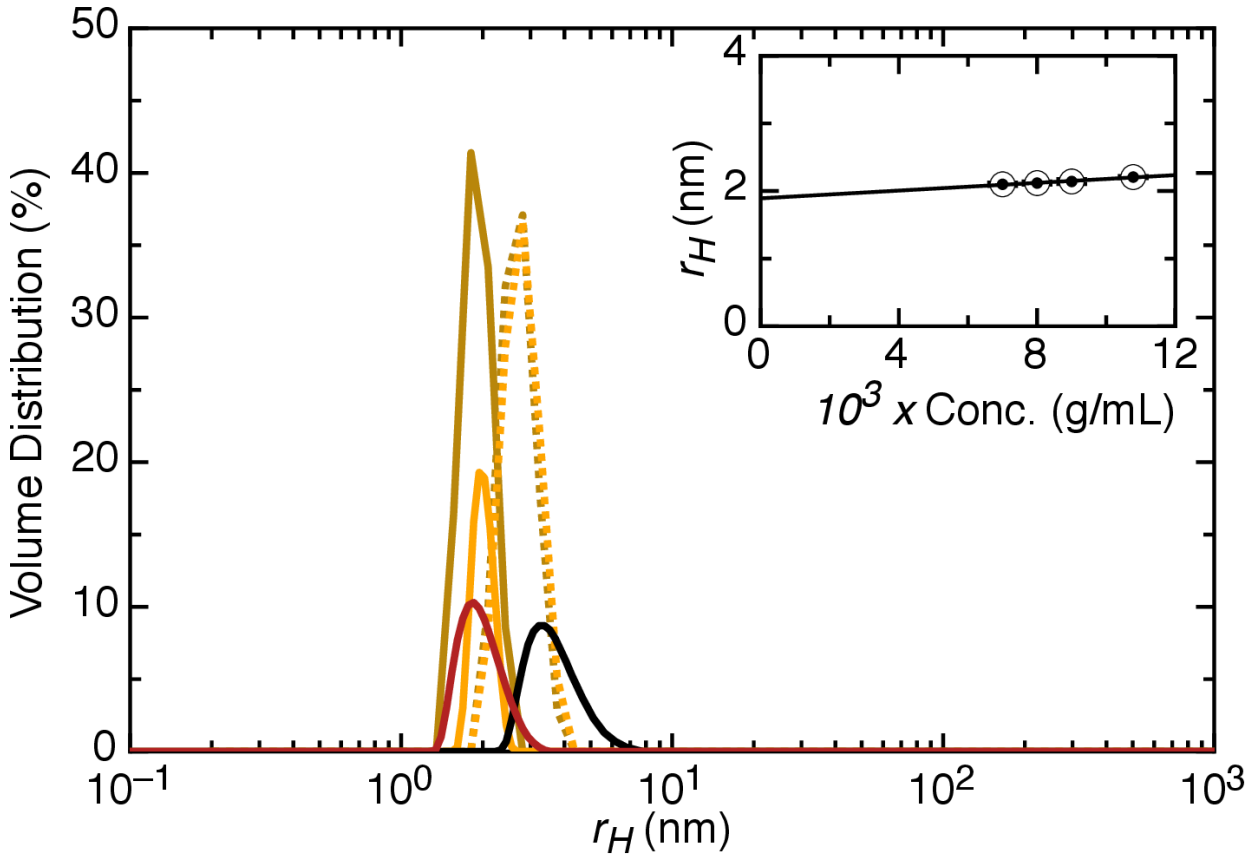

Figure 12. Solution conformation of hTR_{1-20} DNA G-quadruplexes determine by SAXS. A. Scattering profiles of hTR_{1-20} DNA_{c1} (*orange*) and hTR_{1-20} DNA_{c2} (*goldenrod*). The merged measured data for each quadruplex is superimposed with the scattering profiles calculated based on the low resolution models in C. The data was collected in 20 mM HEPES, pH 7.5, I=100 mM (KCl). B. Pair distribution functions for the two G-quadruplexes. C. Average low resolution representations of the G-quadruplexes with D_{max} indicated below the images.

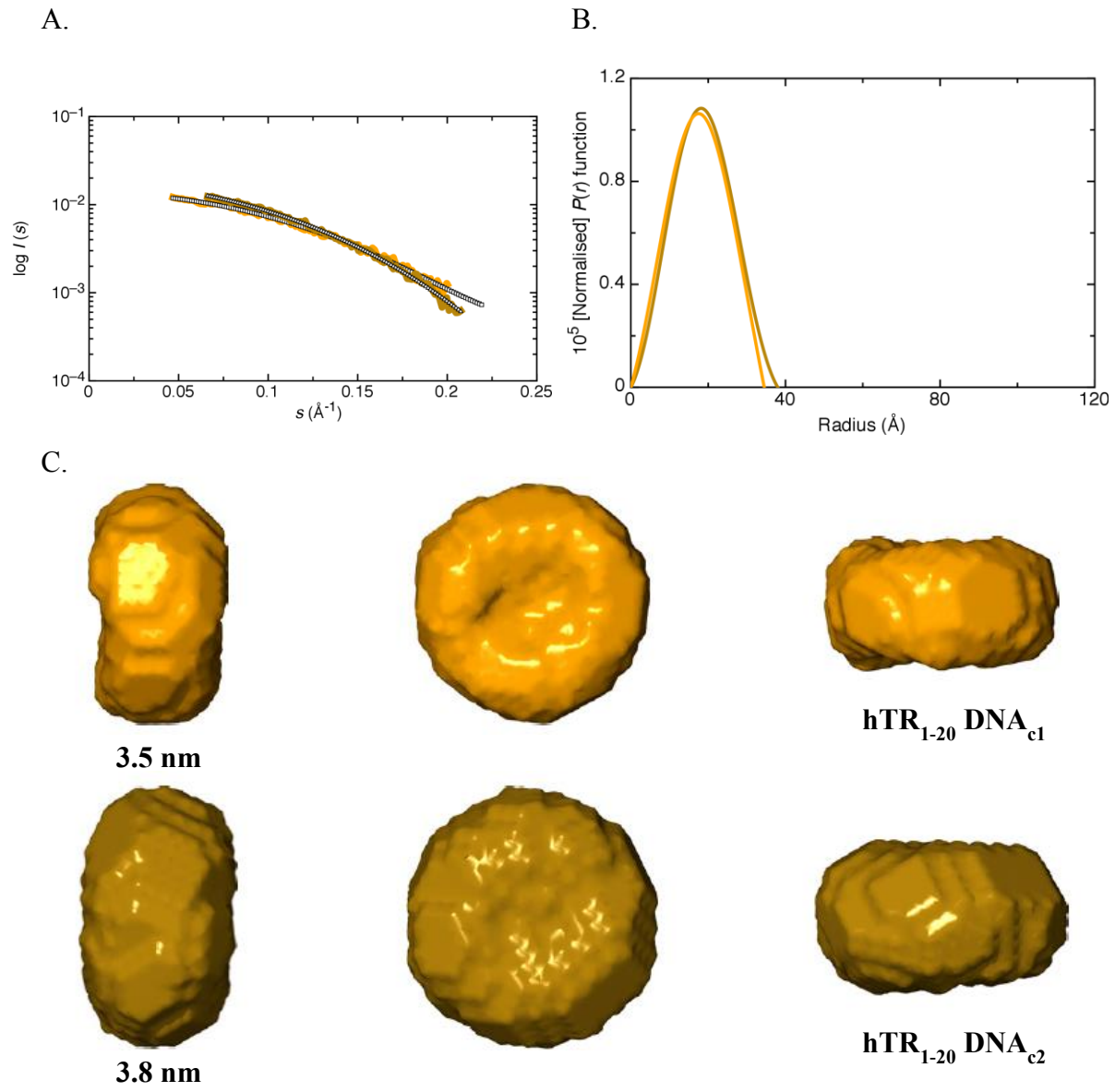

3.2 $RHAU_{53-105}$ ADOPTS EXTENDED CONFORMATION WITH ORDERED SECONDARY STRUCTURE IN SOLUTION

$RHAU_{53-105}$ labelled with an N-terminal His_6 tag expressed in LB media, purified on the Talon® cobalt column and ran as a single band at 8.3 kDa on a denaturing polyacrylamide gel (Figure 13A). Following His_6-tag cleavage with thrombin, $RHAU_{53-105}$, which is 6.4 kDa in size, ran with the 6.5 kDa marker (Figure 13B) and eluted as a single peak in 10 mM HEPES, pH 7.5, I=154 mM (NaCl) from a size exclusion column (Figure 5). The circular dichroism spectrum for $RHAU_{53-105}$ reveals a secondary structure with features of ordered structure and random coil (Figure 14). The CD signal was most prominent in the far UV spectrum and was absent beyond 250 nm. Circular dichroism spectra for $RHAU_{53-105}$ were measured in 10 mM HEPES, pH 7.0, I=154 mM (NaCl), 10 mM TRIS, pH 7.0, I=154 mM (NaCl) and 10 mM sodium phosphate, pH 7.0, I=154 mM (NaF). As shown in Figure 15, the spectra were identical in both HEPES and Tris buffers, but not in sodium phosphate. The proteins aggregated at high concentration in the sodium phosphate buffer, so it was not possible to obtain a meaningful circular dichroism spectrum for $RHAU_{53-105}$ in sodium phosphate below 200 nm. $RHAU_{53-105}$ was analyzed by DLS and SAXS at different concentrations. The protein was found to be monodisperse in solution (Figure 11). The *P(r)* function obtained from the merged scattering profile was used to calculate r_G and D_{max} values of 3.25 (± 0.05) nm and 12.0 nm, respectively (Figure 16A-B, Table 2). The low resolution structure envelope reveals an elongated molecule with two bulges thought to correspond to two subdomains (Figure 16C). The NSD value of 0.51 (±0.02) and χ value of 1.2 presented in Table 1 point to agreement between individually calculated models as well as between experimentally measured and model based hydrodynamic parameters.

Figure 13. Expression and purification of $RHAU_{53-105}$. A. Image of 16% SDS-PAGE gel showing samples collected during expression (*lanes 2-4 from left*) and purification (*lanes 5-11 from left*) of $RHAU_{53-105}$. A band corresponding to $RHAU_{53-105}$ running at 8.3 kDa is present in the samples collected at 2 and 3 hours after induction of expression with IPTG and is absent at 0 hr. The cells were lysed in 20 mM sodium phosphate, 2 mM imidazole, 6 M guanidine hydrochloride, pH 7.0 and purified from the cell lysate by affinity chromatography. $RHAU_{53-105}$ was eluted in 150 mM imidazole, pH 7.0, I=300 mM (NaCl) (*lanes 9-11 from left*). B. Image of 16% SDS-PAGE gel showing $RHAU_{53-105}$ before (*lane 2 from left*) and after (*lane 3 from left*) the cleavage of the N-terminal His_6-tag with thrombin. Following His_6-tag cleavage, the protein was purified on a HiTrap benzamidine FF column (GE Healthcare) to remove thrombin.

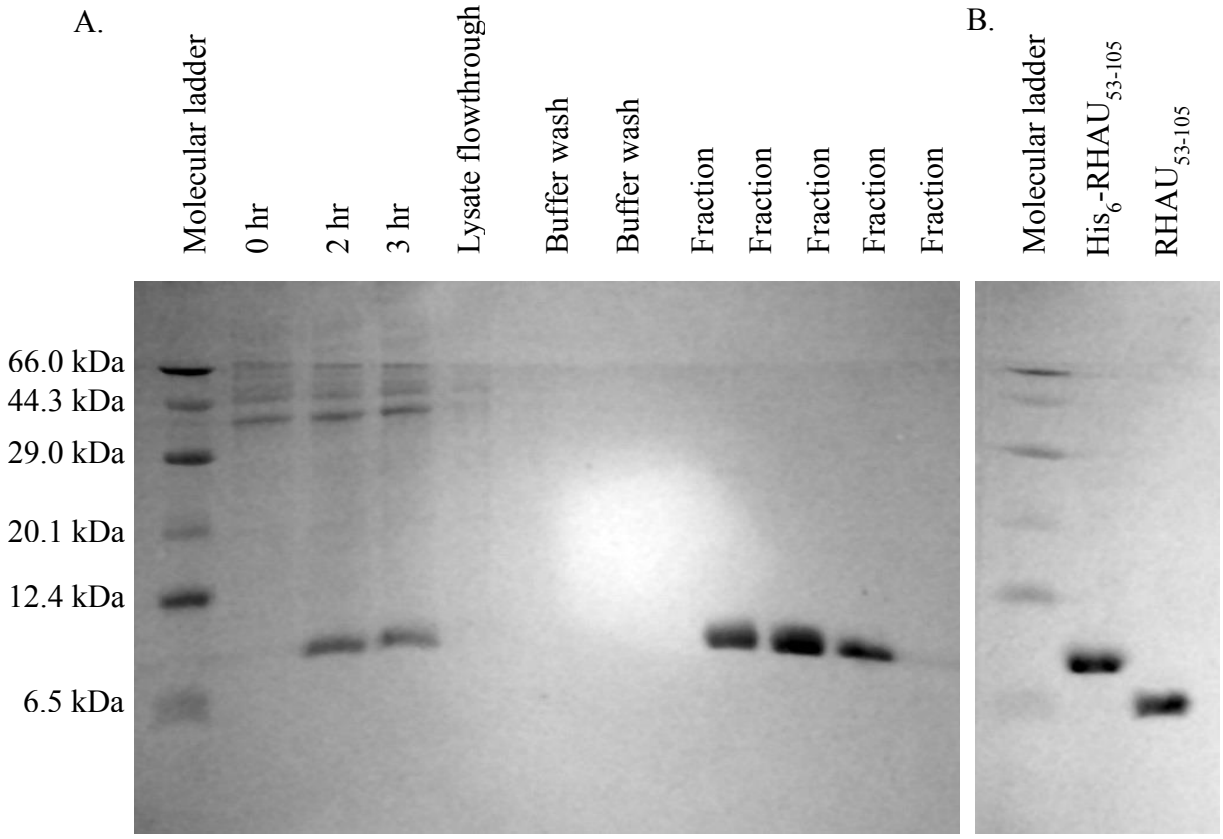

Figure 14. Far UV-visible CD spectrum of $RHAU_{53-105}$. The spectrum was recorded at 20 °C in 10 mM HEPES, pH 7.5, I=154 mM (NaCl). Comparison of the recorded spectrum of $RHAU_{53-105}$ (*red*) with reference spectra of secondary structure elements random coil (rc), α-helix (α) and β-strand (β) reveals evidence of ordered secondary structure in $RHAU_{53-105}$.[77]

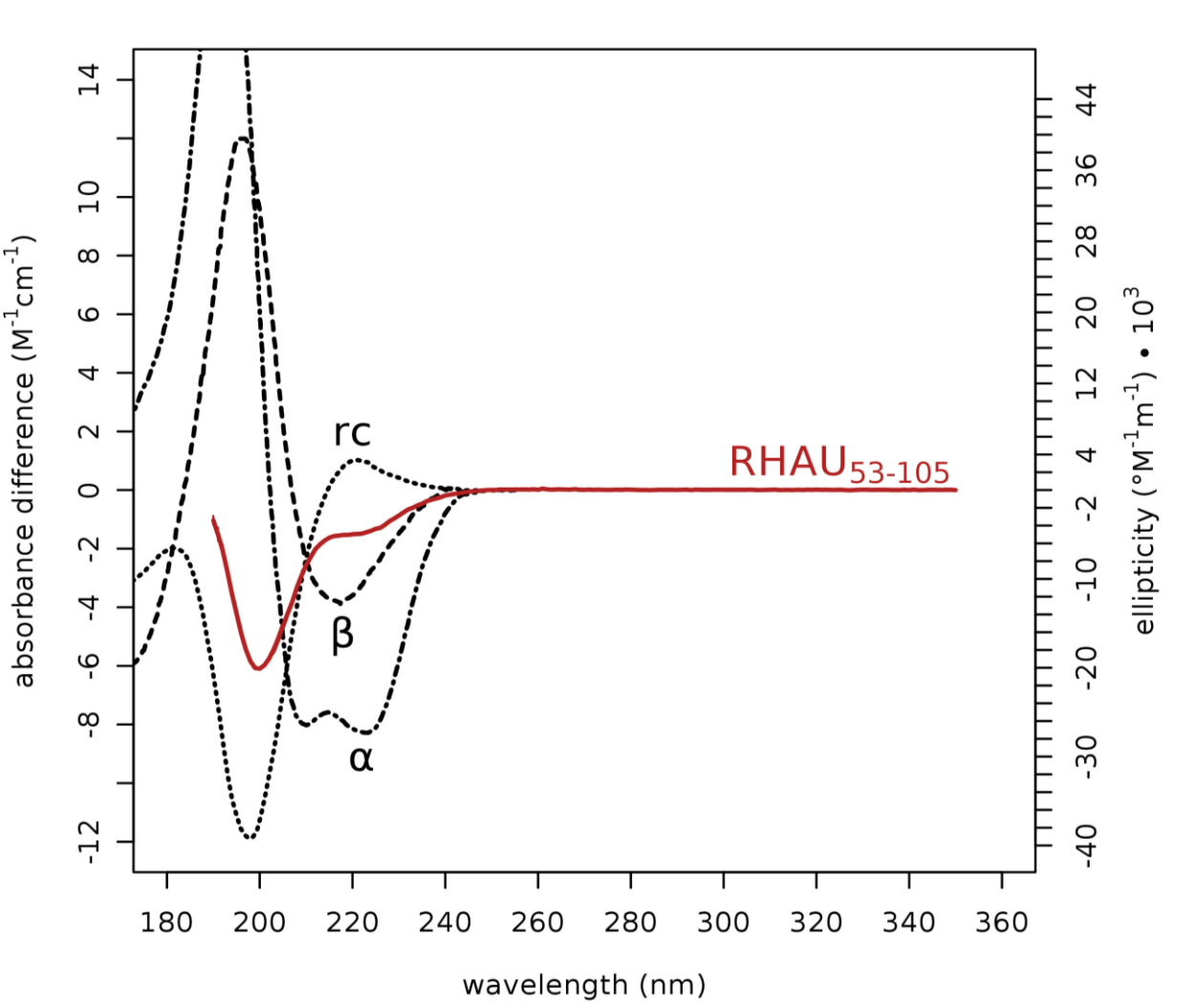

Figure 15. Effect of buffer composition on the conformation of $RHAU_{53-105}$. Circular dichroism spectra for $RHAU_{53-105}$ in 10 mM HEPES, pH 7.0, I=154 mM (NaCl) (*solid line*), 10 mM Tris, I=154 mM (NaCl) (*dashed line*) and 10 mM sodium phosphate, pH 7.0, I=154 mM (NaF) (*dotted line*).

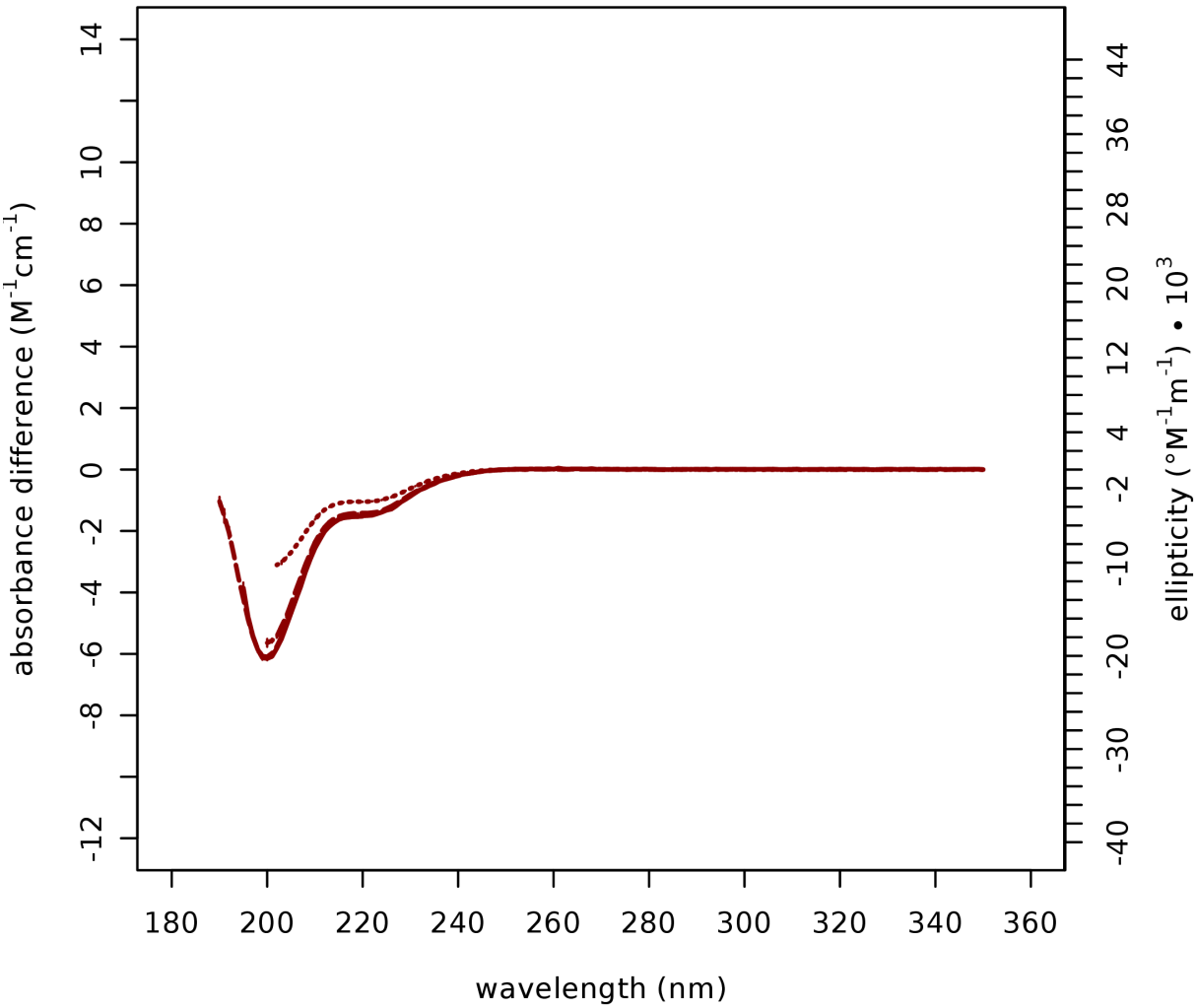

Figure 16. N-terminal domain of RHAU adopts an extended ordered conformation in solution. A. Scattering profiles of $RHAU_{53-105}$ (*red*) and $RHAU_{53-150}$ (*black*). The merged measured data for each RHAU construct is superimposed with the scattering profiles calculated based on the low resolution models in C. The data was collected in 10 mM HEPES, pH 7.5, I=154 mM (NaCl). B. Pair distribution functions for N-terminal RHAU constructs $RHAU_{53-105}$ and $RHAU_{53-150}$ are indicative of extended conformations. C. Average low resolution representations of the N-terminal RHAU constructs with D_{max} indicated beside the images. Superposition of the low resolution models of the two constructs allowed assignment of the N and C termini.

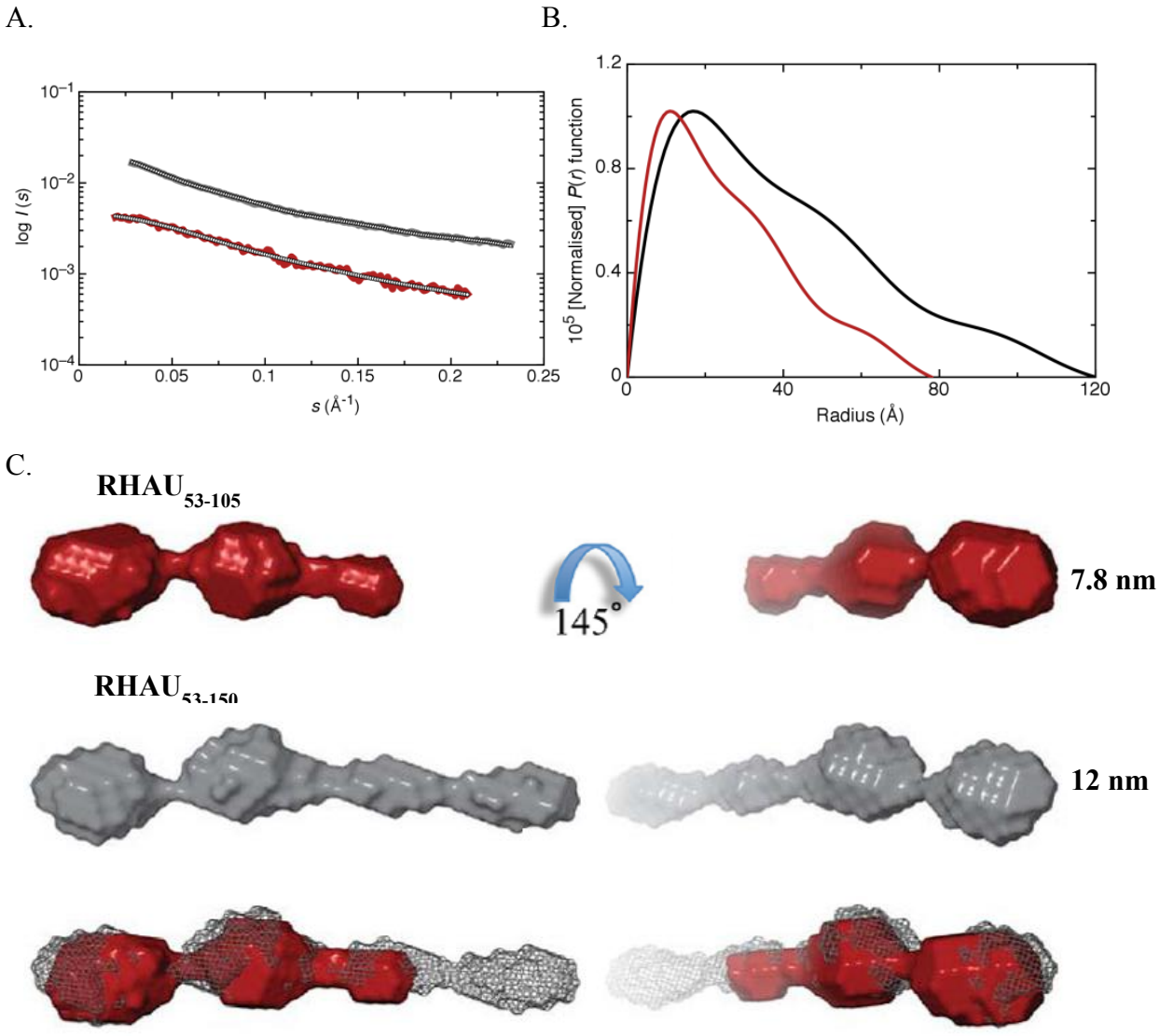

3.3 $RHAU_{53-105}$ BINDS hTR_{1-20} DNA G-QUADRUPLEX IN SOLUTION

The N-terminal construct of RHAU in complex with either hTR_{1-20} DNA_{c1} or hTR_{1-20} DNA_{c2} was analyzed in solution to elucidate the interaction between the RSM of RHAU and G-quadruplex. $RHAU_{53-105}$ was found to shift both hTR_{1-20} DNA_{c1} and hTR_{1-20} DNA_{c2} on a native polyacrylamide gel, suggesting that it binds both DNA quadruplex conformations (Figure 4). In addition, both $RHAU_{53-105}$·hTR_{1-20} DNA_{c1} and $RHAU_{53-105}$·$hTR_{1-20}DNA_{c2}$, each mixed in 1:1 molar ratios, eluted as single peaks from a size exclusion chromatography column (Figure 5). CD spectra obtained for both complexes are shown in Figure 17 along with the spectra for G-quadruplexes alone. The CD signal was influenced by both the protein component and the quadruplex below 250 nm and only the quadruplex component dominated the spectrum above 250 nm. The wavelengths of the maxima and minima remained unchanged from those observed for quadruplexes alone, but the horizontal shoulder to the right of the 263 nm maximum in hTR_{1-20} DNA_{c2} was transformed to a sloped shoulder in the complex of hTR_{1-20} DNA_{c2} and $RHAU_{53-105}$. SAXS data was collected for each complex at a range of concentrations and the merged scattering profiles (Figure 18A) were used to obtain two bell-shaped *P(r)* functions (Figure 18B). The low resolution structures appear as globular shapes without defined subdomains (Figure 14C). D_{max} values of 5.0 nm for $RHAU_{53-105}$·hTR_{1-20} DNA_{c1} and 5.2 nm for $RHAU_{53-105}$·hTR_{1-20} DNA_{c2} show that both complexes assume a compact conformation relative to the extended structure of $RHAU_{53-105}$ alone. The hydrodynamic parameters summarized in Table 1 are similar for both complexes. The NSD ($\leq$0.56 for both complexes) and χ (1.1 and 1.2 for complex with hTR_{1-20} DNA_{c1} and hTR_{1-20} DNA_{c2}, respectively) values reveal agreement between individual models used to calculate the merged average model for each complex as well as between experimentally derived and model-based parameters. DLS measurements (Figure 11) obtained

before and after SAXS data collection show the presence of monodisperse molecule in solution and absence of observable radiation damage after exposure to X-rays.

Figure 17. Conformational change associated with protein binding to DNA G-quadruplex. Far UV-visible CD spectra of hTR_{1-20} DNA_{c1} (*orange, solid*) and hTR_{1-20} DNA $_{c2}$ (*goldenrod, solid*) to $RHAU_{53-105}$·hTR_{1-20} DNA_{c1} (*orange, dotted*) and $RHAU_{53-105}$·$hTYR_{1-20}$ DNA_{c2} (*goldenrod, dotted*) were obtained at 20 °C in 20 mM HEPES, pH 7.5 and I=100 mM (KCl).

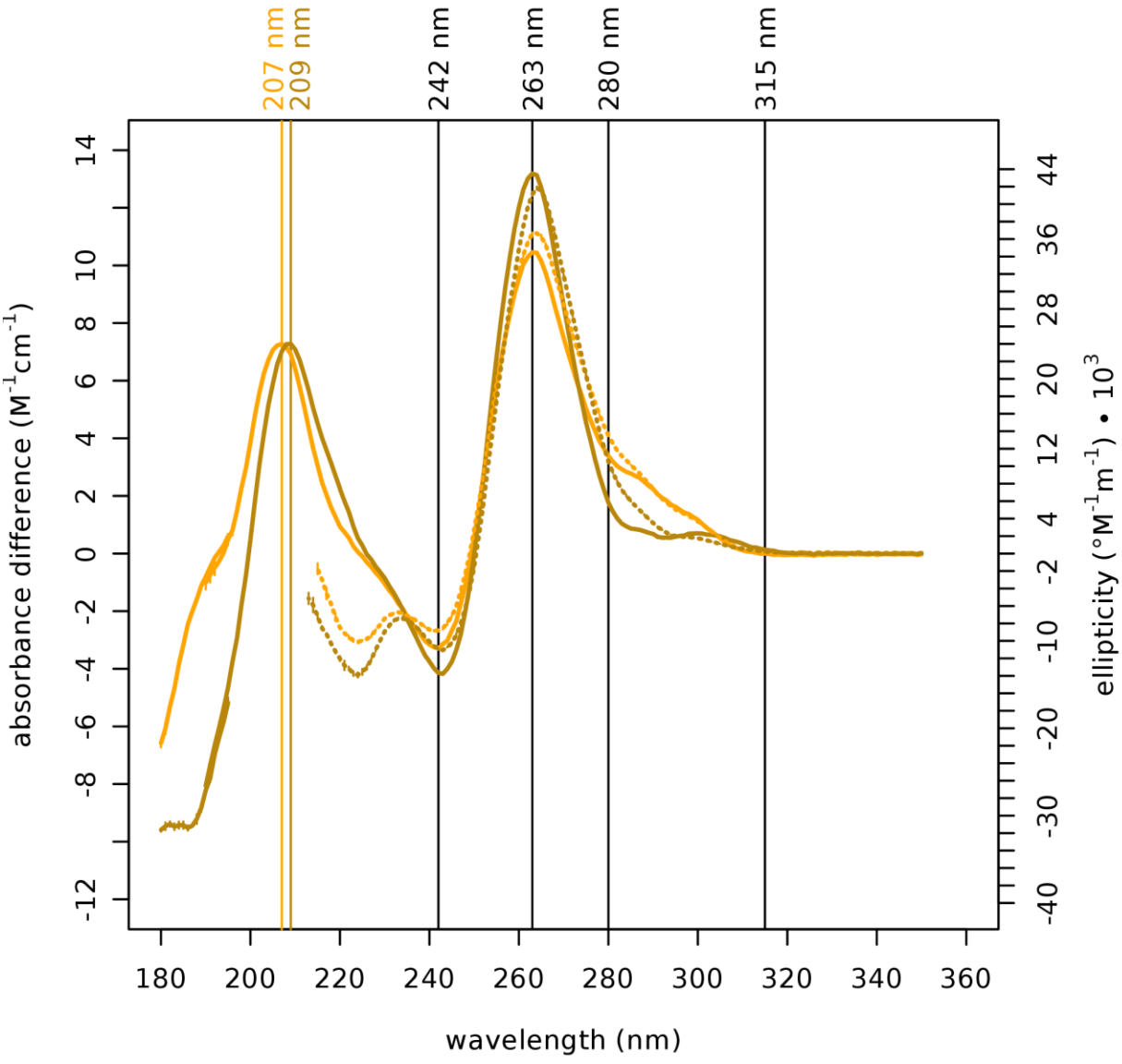

Figure 18. Solution conformations of G-quadruplex-protein complexes determined by SAXS. A. Scattering profiles of $RHAU_{53\text{-}105}$·$hTR_{1\text{-}20}$ DNA_{c1} (*orange*) and $RHAU_{53\text{-}105}$·$hTR_{1\text{-}20}$ DNA_{c2} (*goldenrod*). The merged measured data for each complex is superimposed with the scattering profiles calculated based on the low resolution models in C. The data for each complex was collected in 20 mM HEPES, pH 7.5, I=100 mM (KCl). B. Pair distribution functions for the two complexes. C. Average low resolution representations of the protein-G-quadruplex complexes with D_{max} indicated beside the images.

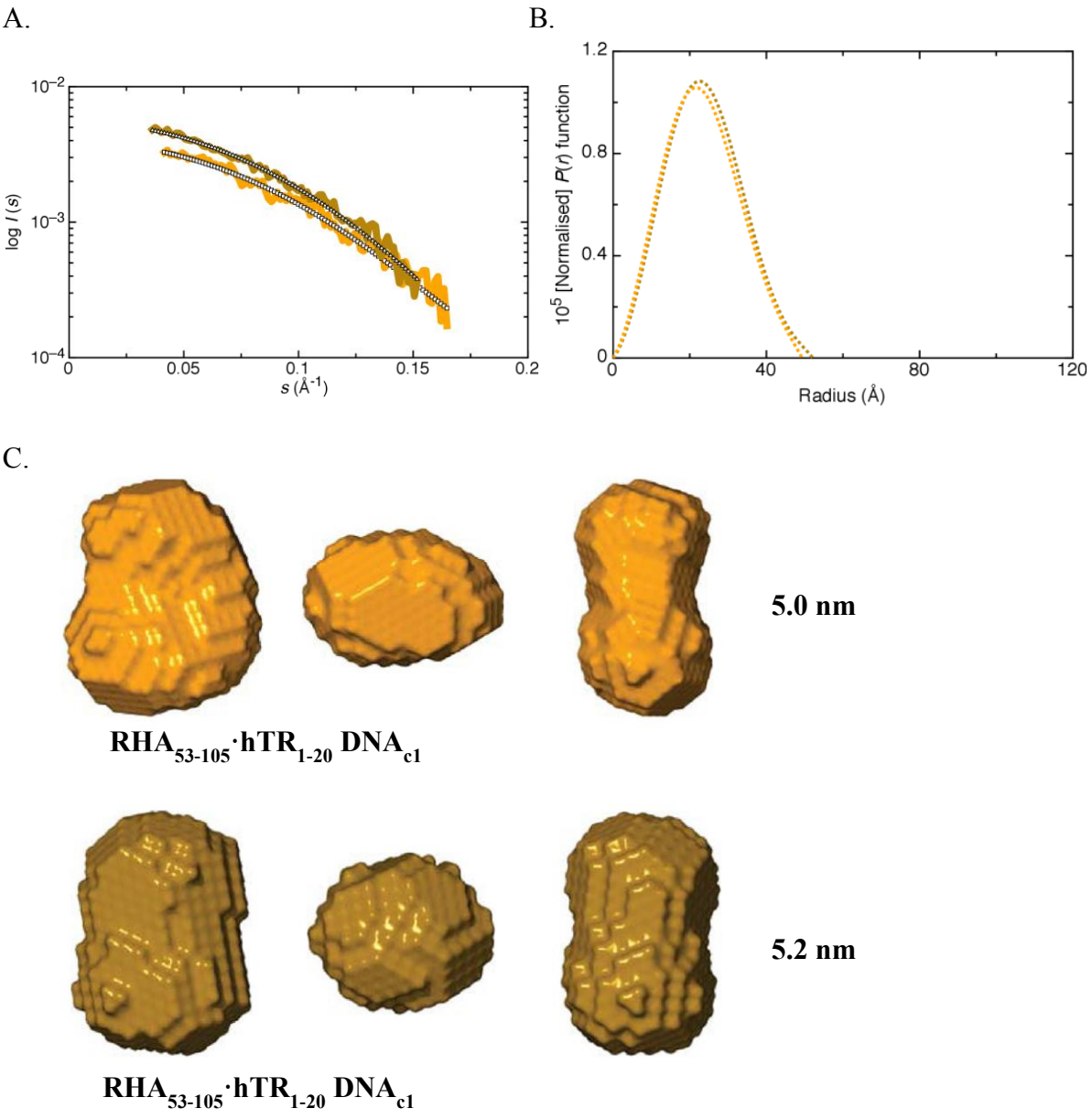

Table 2. Summary of hydrodynamic data for the protein, quadruplexes and complexes. Errors are indicated in the parenthesis and dashes indicate values that could not be determined.

	$RHAU_{53-105}$		$hTR_{1-20}\,DNA_{c1}$		$hTR_{1-20}\,DNA_{c2}$	
Hydrodynamic parameter	Experimental	Model-based[d]	Experimental	Model-based[d]	Experimental	Model-based[d]
r_H(nm)[a]	1.90 (±0.03)	2.00 (±0.02)	1.90 (±0.02)	1.83 (±0.04)	1.90 (±0.07)	1.95 (±0.08)
r_G(nm)[b]	2.1 (±0.2)	2.2 (±0.2)	1.34 (±0.06)	1.48 (±0.07)	1.41 (±0.08)	1.57 (±0.01)
D_{max}(nm)[c]	7.8	8.1 (±0.1)	3.5	3.8 (±0.04)	3.8	4.00 (±0.04)
r_G/r_H	1.1 (±0.2)	1.1 (±0.2)	0.71 (±0.08)	0.81 (±0.08)	0.7 (±0.1)	0.8 (±0.1)
χ	-	1.1	-	0.8	-	0.9
NSD	-	0.58 (±0.06)	-	0.50 (±0.01)	-	0.51 (±0.02)

	$RHAU_{53-105}\cdot hTR_{1-20}\,DNA_{c1}$		$RHAU_{53-105}\cdot hTR_{1-20}\,DNA_{c2}$	
Hydrodynamic parameter	Experimental	Model-based[d]	Experimental	Model-based[d]
$r_H(nm)_a$	2.7 (±0.1)	2.4 (±0.1)	2.70 (±0.07)	2.5 (±0.1)
r_G(nm)[b]	1.78 (±0.02)	1.9 (±0.1)	1.82 (±0.01)	2.0 (±0.1)
D_{max}(nm)[c]	5.0	5.5 (±0.05)	5.2	5.60 (±0.05)
r_G/r_H	0.7 (±0.1)	0.8 (±0.2)	0.67 (±0.08)	0.8 (±0.2)
χ	-	1.2	-	1.1
NSD	-	0.56 (±0.02)	-	0.5 (±0.01)

[a] The values were experimentally determined from DLS data with error obtained from linear regression analysis to infinite dilution for multiple concentrations.
[b] The values were experimentally determined from the SAXS data with error obtained from *P(r)* analysis by GNOM.
[c] The values were experimentally determined from SAXS data obtained from *P(r)* analysis by GNOM.
[d] Model-based parameters calculated from HEDROPRO with errors obtained as the S.D. from multiple models.

3.4 CRYSTALLIZATION TRIALS

Commercial crystallization screens Crystal Screen HT and Natrix HT (Hampton Research, CA, USA) were used to test one hundred ninety-two crystallization solutions for a condition suitable for crystallization of hTR_{1-20} DNA quadruplexes. Conformation 1 of hTR_{1-20} DNA did not yield any crystals. In contrast, fine needle-like crystals appeared in the drop of hTR_{1-20} DNA_{c2} at 5.41 mg/ml with 0.4 M potassium sodium tartrate tetrahydrate. The crystals, pictured in Figure 19, were first observed two months after the crystal screens were set-up. Because the crystals were too small to mount, they were not tested for X-ray diffraction.

Commercial crystallization screens Crystal Screen HT, Natrix HT, PEG/ION HT and Index HT (Hampton Research, CA, USA) were used to check three hundred eighty-four solutions for conditions appropriate for crystallization of the $RHAU_{53-105}$·hTR_{1-20} DNA quadruplex complexes. The complex of $RHAU_{53-105}$ and hTR_{1-20} DNA_{c1} was tested at two concentrations (5.09 mg/ml and 8.65 mg/ml protein), but no crystals were obtained. In contrast, due to limited availability of hTR_{1-20} DNA_{c2}, hTR_{1-20} DNA_{c2}·$RHAU53_{-105}$was only tested at 5.41 mg/ml (protein concentration). The following four conditions in the PEG/ION HT screen produced crystals: 0.2 M sodium formate, 20 % w/v PEG 3350; 0.2 M potassium formate, 20 % w/v PEG 3350; 0.2 M ammonium formate, 20 % w/v PEG 3350 and 0.2 M sodium formate pH 7.0, 20 % w/v PEG 3350. All crystals had the shape of rectangular prisms with smooth faces, but they dissociated into clusters of fine needle-like crystals upon removal of the protective film from the top of the well to check the crystals for X-ray diffraction. Figure 20A shows the image of the crystals obtained in 0.2 M sodium formate, 20 % w/v polyethylene glycol (PEG) 3350 after the well had been opened. To verify whether the crystals were composed of the protein-DNA complex or salt, an X-ray diffraction pattern was obtained (Figure 20B). The crystal was

cryoprotected in 24% PEG 3350 and 10 % ethylene glycol and its ability to diffract X-rays was tested at three angles, for ten minutes at each angle. The diffraction pattern presented in Figure 20B shows that although the crystal diffracted to as far as 4.1 Å, the spots are smeared and weak, likely due to the dispersion of the original crystal into parallel fine needle-like crystals. The attempt to optimize the conditions with PEG 3350 in order to obtain crystals less prone to dissociation failed.

A subsequent screen of $RHAU_{53\text{-}105}{\cdot}hTR_{1\text{-}20}$ DNA_{c2} at 4.0 mg/ml (protein component) using commercial kits Crystal Screen 1 and Crystal Screen 2 (Hampton Research, CA, USA) identified 1.5 M sodium chloride, 10 % v/v ethanol as a promising condition for crystallization of this complex. The crystal appeared two weeks after the screens were set-up. The crystal, shown in Figure 21A, appears to be composed of numerous microcrystals, so further optimization is necessary. Nevertheless, it stains with methyl blue (Figure 22B), suggesting it contains protein.

Figure 19. Image of crystals of $hTR_{1\text{-}20}$ DNA_{c2} grown by vapour diffusion in 0.4 M potassium sodium tartrate tetrahydrate at 20 °C. Sitting drops were prepared by adding 1 µL of the reservoir solution to 1 µL of $hTR_{1\text{-}20}$ DNA_{c2} at 7.26 mg/ml. The well contained 50 µl of the reservoir solution. The observed crystals appeared after two months.

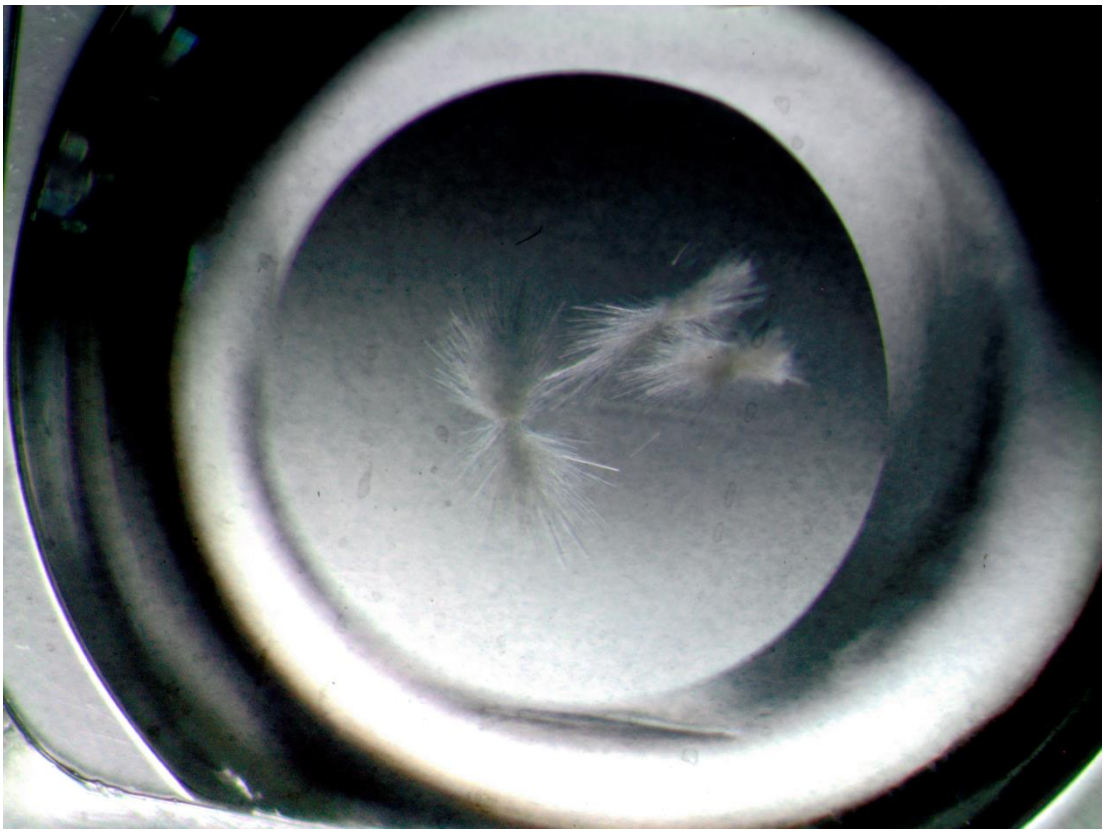

Figure 20. A. Image of crystals of hTR_{1-20} DNA_{c2}·$RHAU_{53-105}$ grown by vapour diffusion in 0.2 M sodium formate, 20 % w/v polyethylene glycol 3350. Sitting drops were prepared by adding 1 µL of the reservoir solution to 1 µL of the complex (5.41 mg/ml protein concentration in complex). The well contained 50 µl of the reservoir solution. The observed crystals appeared after two months. B. X-ray diffraction pattern obtained for crystal shown in A after exposure to X-rays for 10 minutes. The crystal was cryoprotected in 24% polyethylene glycol 3350 and 10 % ethylene glycol. The resolution is 4.1 Å.

A

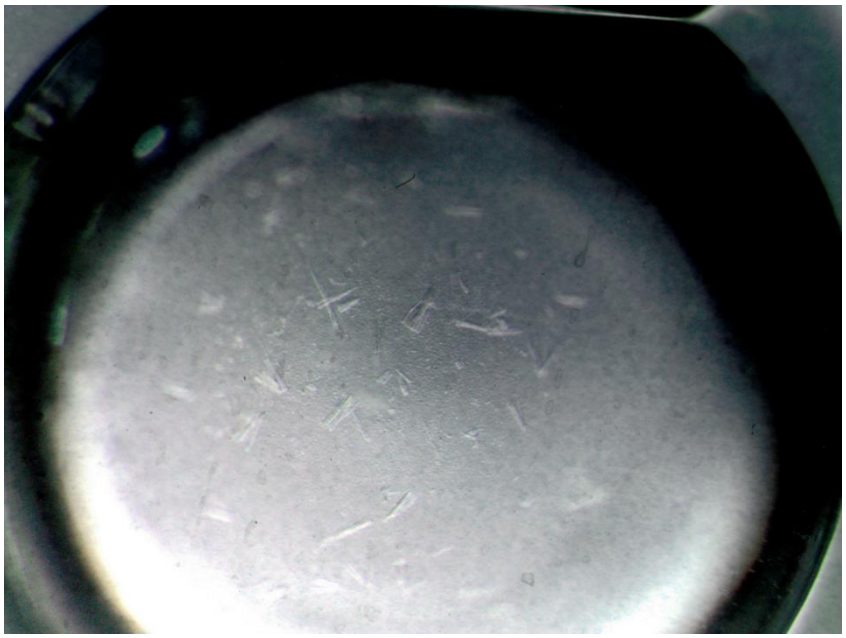

B

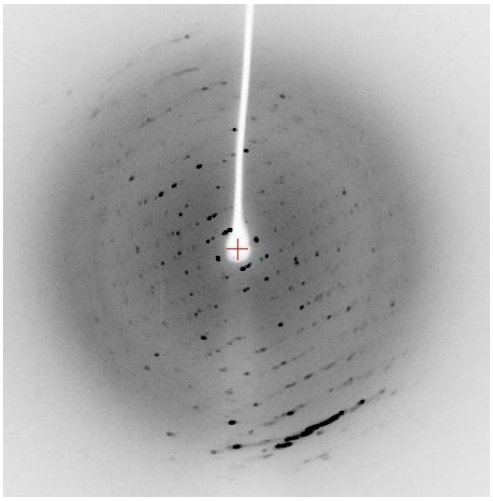

Figure 21. A. Image of crystals of $hTR_{1\text{-}20}$ DNA_{c2}·$RHAU_{53\text{-}105}$ grown by vapour diffusion in 1.5 M sodium chloride, 10 % v/v ethanol. Hanging drops were prepared by adding 2 µL of the reservoir solution to 2 µL of the complex (4.00 mg/ml protein concentration in complex). The well contained 1.00 mL of the reservoir solution. The observed crystals appeared after two weeks. B. The crystals stain with methyl blue.

A

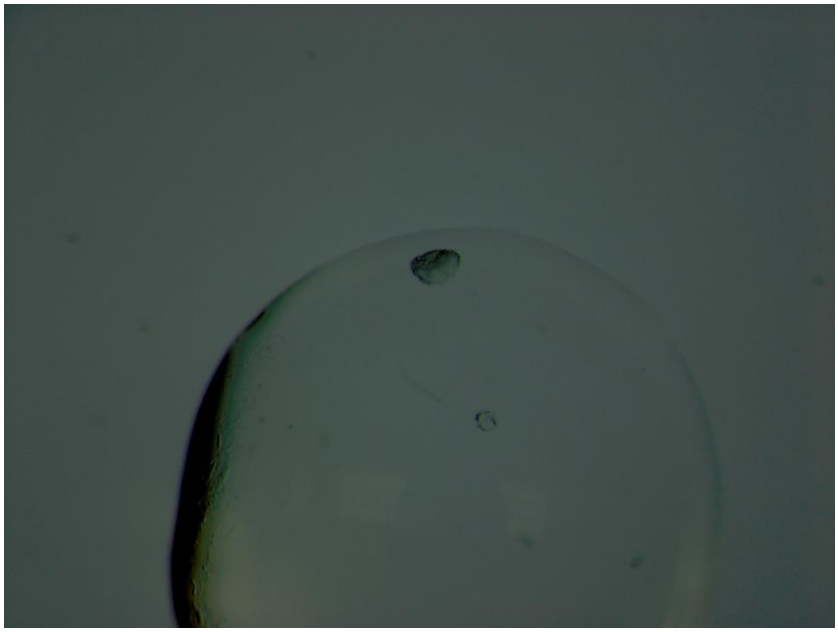

B

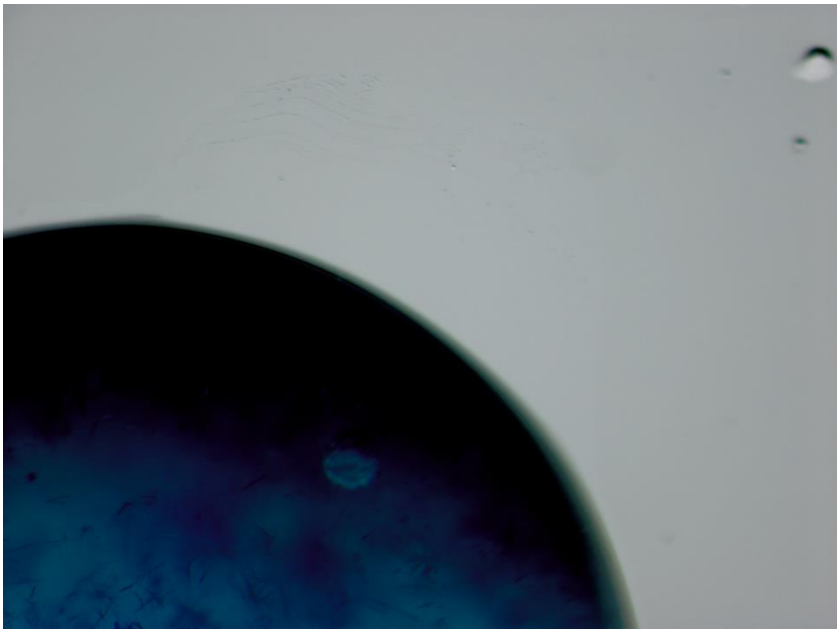

3.5 EXPRESSION AND PURIFICATION OF THE FULL-LENGTH RHAU PROTEIN

In order to extend the biophysical analysis to the full length RHAU protein, expression of His_6-$RHAU_{53-1008}$ was attempted in *E. coli*. $RHAU_{53-1008}$ is 110 kDa in size and, except for the first N-terminal fifty-two amino acids, represents the full length RHAU protein. The glycine-rich N-terminus is predicted to be disordered and was omitted due to concern over its ability to crystallize. The initial effort to express His_6-tagged construct of the RHAU protein composed of amino acids 53 to 1008 in *E. coli* strain BL21(DE3) was unsuccessful (Figure 22A). To aid in expression, the His_6-$RHAU_{53-1008}$.pET-15b plasmid was transformed into *E. coli* strain BL21(DE3)-RIPL, which corrects for the codon bias in *E.coli* with extra copies of *argU, ileY, leuW* and *proL* tRNA genes. A band running immediately above the 100 kDa marker, comparable to the expected size of His_6-$RHAU_{53-1008}$, is evident in samples collected from the BL21(DE3)-RIPL culture, suggesting that $RAHU_{53-1008}$ was produced (Figure 22B). Then, purification was attempted by affinity chromatography using Ni-NTA agarose beads. Although RHAU protein was detected in the cell lysate (Figure 23), it was not present in any of the imidazole buffers used to wash the beads following incubation with the lysate in an attempt to elute any bound protein. Some RHAU protein was also detected in washing buffer fractions at the very top of the gel, suggesting that RHAU might have aggregated.

In an effort to produce the RHAU protein in a eukaryotic system, such as Human Embryonic Kidney 293T (HEK293T) cells, $RHAU_{53-1008}^{\Delta 14}$ was cloned in the pCEP-Pu.BM40 vector optimized for overexpression of proteins in HEK293T cells. The $RHAU_{53-1008}^{\Delta 14}$ construct is missing the nuclear localization signal located at amino acids 516 to 529. The nuclear localization signal was removed because it would have competed with the extracellular secretion signal contained in the pCEP-Pu.BM40 vector.

Figure 22. Expression of $RAHU_{53-1008}$ in *Escherichia coli* cells. A. Samples collected during expression of His_6-tagged $RHAU_{53-1008}$ in *E. coli* strain BL21(DE3) cells. The samples were mixed with reducing Laemmli buffer and heated at 95 °C for 4 minutes before loading on the gel. B. After induction of expression of His_6-tagged $RHAU_{53-1008}$ in *E. coli* strain BL21(DE3)-RIPL cells with IPTG, samples were collected every thirty minutes for two hours. The samples were mixed with 10% sodium dodecyl sulfate and reducing Laemmli buffer in a 1:1 tio and heated at 95 °C for 4 minutes before loading on the gel.

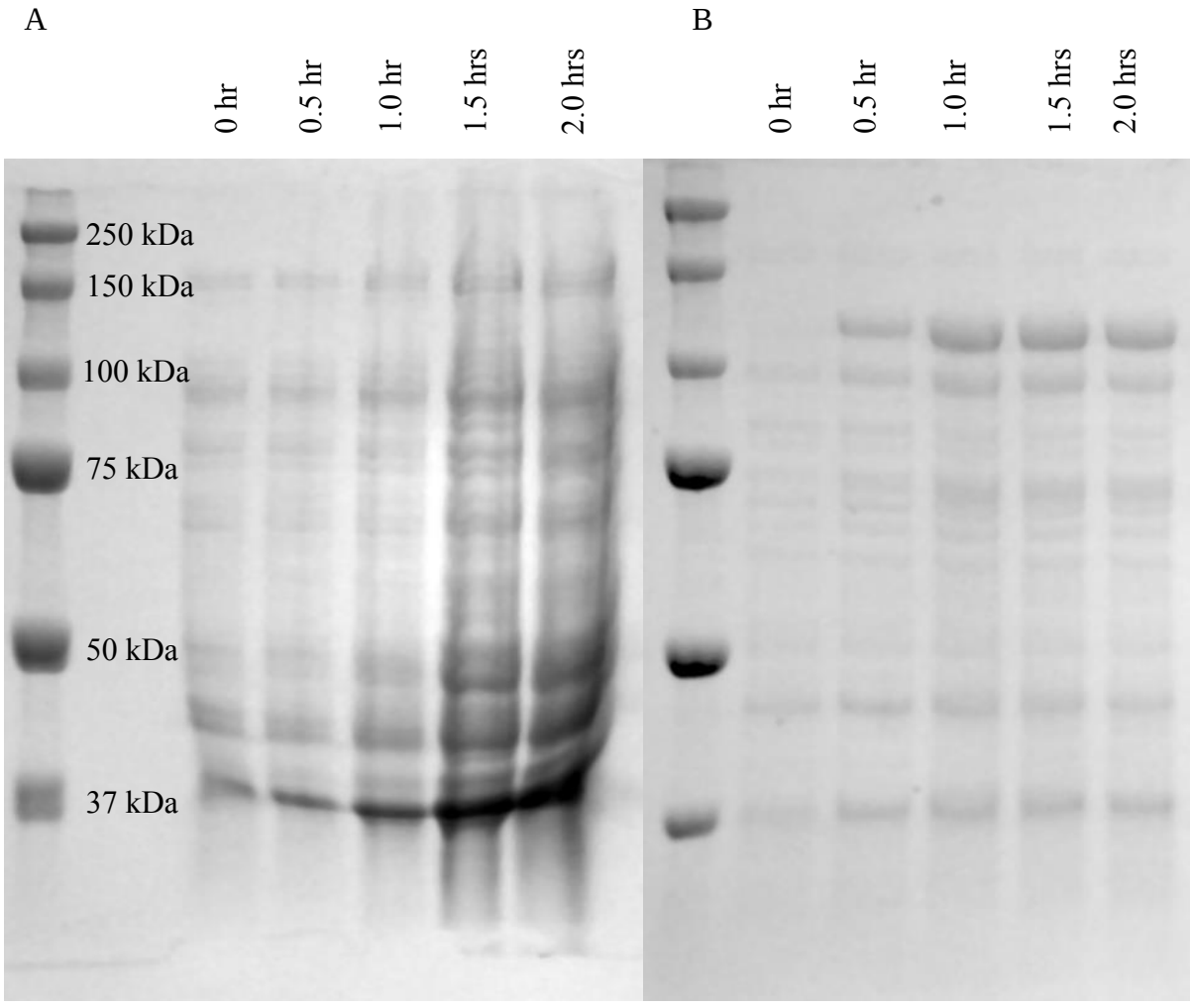

Figure 23. A. Purification of His_6-$RHAU_{53-1008}$ expressed in *Escherichia coli* BL21(DE3)-RIPL cells. A. An image of a 10% polyacrylamide gel resolved by electrophoresis showing the cell lysate and the fractions collected during purification of His_6-tagged $RHAU_{53-1008}$ protein by batch purification with nickel beads. The purification procedure was carried out under native conditions and protein elution was attempted with imidazole gradient. B. Western Blot for $RHAU_{53-1008}$ superimposed over the gel shown in A. $RAHU_{53-1008}$, indicated by the black arrow, was detected using a mouse anti-RAHU primary antibody and horse radish peroxidase conjugated anti-mouse secondary antibody.

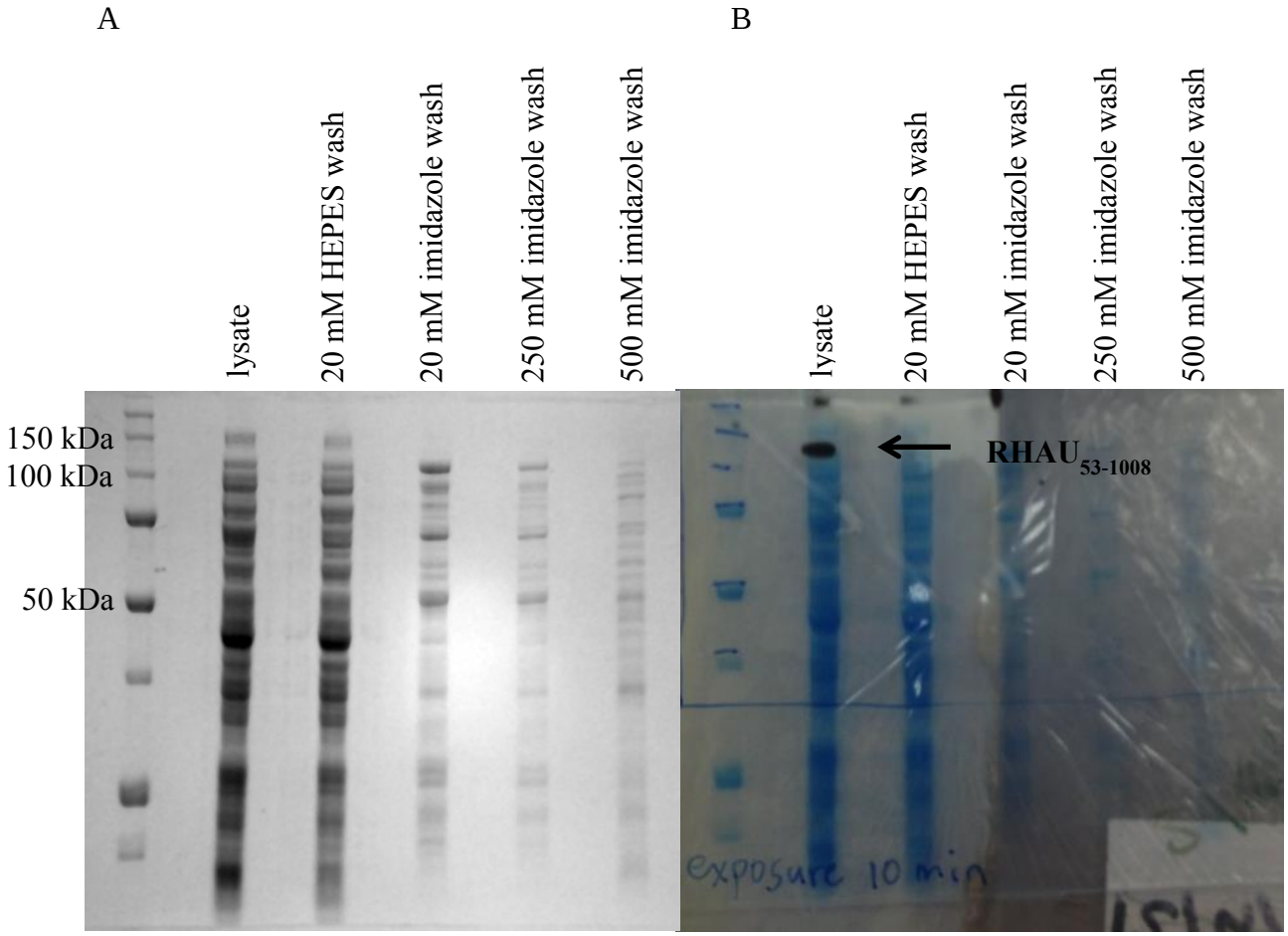

4. Discussion

G-quadruplexes have been identified in key areas of the human genome, including telomeres, promoter regions of genes and 5' and 3'-UTRs of mRNAs.[6,18,22,24–26,78] Non-random distribution of G-rich sequences potentially capable of forming G-quadruplexes suggests that these structures are of physiological importance to gene metabolism.[22] In fact, G-quadruplexes have been implicated in transcriptional and translational regulation, gene splicing, and disease.[20] These highly stable structures must be unwound to allow for correct functioning of the genome. Although unwinding of double-stranded oligonucleotides has been studied in detail, little information is available about quadruplex recognition and unraveling. To date, RHAU has been identified as a major ATP-dependent G-quadruplex resolvase in human cells.[52] The conserved N-terminal RSM motif was shown to be required for quadruplex recognition and binding, but not for quadruplex unwinding.[56,79] Although RHAU has been shown to bind both DNA and RNA G-quadruplexes *in vitro,* its main target in cell lysate was found to be a G-quadruplex in the 5' terminus of hTR.[52,53,55,56] The sequence upstream of the P1 helix in hTR contains several guanine runs and can form G-quadruplexes thought to serve a protective function during TERT maturation.[56] The P1 helix, conserved among all known vertebrates except rodents, is a structural element required for boundary definition of the telomere RNA template sequence and its formation may be impeded by incorporation of nucleotides required for its assembly into upstream G-quadruplex structures.[58,59]

The binding between an N-terminal construct of RHAU and the DNA quadruplexes formed by the hTR_{1-20} sequence was investigated using an integrated biophysical approach. $RHAU_{53-105}$ and two conformations of the quadruplex were purified and were used to prepare $RHAU_{53-105}$·hTR_{1-20} DNA complexes in a 1:1 molar ratio. A DNA analog of the hTR_{1-20}

sequence was used in this analysis to compare the structural features of the hTR_{1-20} quadruplex to its DNA analogs and to determine whether the DNA analogs would be suitable for subsequent use in X-ray crystallography. The hTR_{1-20} DNA was purified in two conformations in the presence of potassium cations. Since both conformations are of the same molecular weight, they likely fold differently from each other, resulting in a larger solvated volume for conformation 1. In fact, conformation 1 elutes prior to conformation 2 from a size exclusion column. The presence of quadruplex secondary structure was confirmed by CD, hypochromicity measurements, SAXS and staining with quadruplex specific dye N-methylmesoporphyrin IX. Hypochromicity of 30.9% and 37.5% was observed for hTR_{1-20} DNA_{c1} and hTR_{1-20} DNA_{c2}, respectively, at 297 nm at 80°C relative to 20°C. Such significant decrease in absorbance at 297 nm is indicative of G-quadruplex unfolding and is associated with the helix-coil transition.[80] High melting temperatures (~70 °C for hTR_{1-20} DNA_{c1} and~ 64 °C for hTR_{1-20} DNA_{c2}) further confirm that hTR_{1-20} DNA assumes a G-quadruplex secondary structure in solution. These temperatures are higher than the melting temperature of double-stranded DNA helix, although they are lower than the 80 °C obtained for the melting temperature of the hTR_{1-20} RNA G-quadruplex.[81]

The possibility of interconversion between the two conformations of the hTR_{1-20} DNA G-quadruplex was investigated by SEC, UV-Vis spectrophotometry and spectropolarimetry. After a heating-cooling cycle, a portion of conformation 1 was shown to refold into conformation 2, although the portion of conformation 2 formed decreased with each successive heating-cooling cycle. This finding suggests that hTR_{1-20} DNA_{c1} might be a mixture of more than one conformation that due to their similarities cannot be easily resolved on a HiLoad Superdex 75 26/60 column (GE Healthcare). In contrast, hTR_{1-20} DNA_{c2}, which makes up about one-third of

the hTR_{1-20} DNA after the first heating-cooling cycle, does not change its conformation following additional heating and cooling. No interconversion of hTR_{1-20} DNA_{c2} to hTR_{1-20} DNA_{c1} was detected by either UV-Vis spectrophotometry or spectropolarimetry.

The two conformations of the quadruplex were differentiated by spectropolarimetry. The CD spectra for both hTR_{1-20} DNA conformations are characteristic of parallel quadruplexes with characteristic maximum and minimum at ~260 nm and ~240 nm, respectively. In contrast, CD spectra for anti-parallel quadruplexes typically display a maximum at ~290 nm and a minimum at ~260 nm.[82] In addition, the N-methylmesoporphyrin IX compound used to stain the hTR_{1-20} DNA has previously been shown to be specific to parallel quadruplexes.[11]

Recent analysis of a shorter 5' hTR sequence, hTR_{1-18}, in 100 mM K^+ reveals similar findings regarding its conformation in solution.[7] Martadinata *et al*. studied hTR_{1-18} by gel electrophoresis, UV, CD and NMR, although they did not present a high resolution structure of the quadruplex.[7] In addition, they show that the quadruplexes formed by hTR_{1-18} likely dimerize in solution by stacking at their 5' termini.[7] Since hTERT has been shown to function as a dimer *in vivo*, the authors suggest that the observed quadruplex stacking might be involved in dimerization of TERT.[7,83]

The hTR_{1-20} alone and in complex with $RHAU_{53-105}$ was separately analysed in a comprehensive biophysical approach.[81] The RNA quadruplex formed by hTR_{1-20} assumed a single conformation in the presence of potassium cations. Like the two conformations of the hTR_{1-20} DNA quadruplex, the hTR_{1-20} quadruplex exhibits a minimum at 242 nm, although the maximum for the RNA occurs at 264 nm instead of 263 nm.[81] The hydrodynamic parameters obtained for the DNA quadruplexes are similar to the parameters of the hTR_{1-20} quadruplex for which r_H, r_G and D_{max} were found to be 1.91 (±0.02) nm, 1.31 (±0.08) nm and 3.4 nm,

respectively. As for the DNA quadruplexes, the SAXS envelope for hTR_{1-20} has a disk-like shape with two concave faces. However, the hTR_{1-20}·$RHAU_{53-105}$ complex appears to be more extended (r_H = 3.10 (±0.05) nm, r_G = 2.60 (±0.04) nm and D_{max} = 8.5 nm) than either hTR_{1-20} DNA_{c1}·$RHAU_{53-105}$ or hTR_{1-20} DNA_{c2}·$RHAU_{53-105}$ complex. The SAXS envelope for the hTR_{1-20}·$RHAU_{53-105}$ complex appears similar to the low resolution model for $RHAU_{53-105}$ alone, except the N-terminal region of the RHAU construct is enlarged. NMR analysis reveals the perturbation of same backbone residues in $RHAU_{53-105}$ upon binding to either hTR_{1-20} or hTR_{1-20} DNA analogs, suggesting that the 2'-OH group of RNA is not required for binding to RSM of RHAU.[81] However, the absence of the 2'-OH group in hTR_{1-20} DNA quadruplex likely permits an interaction between the quadruplex and a region of $RHAU_{53-105}$ downstream of the RSM, accounting for the compact shape of the low resolution models calculated for the hT_{R1-20} DNA-$RHAU_{53-105}$ complexes based on SAXS data.[81] This structure reveals that the N-terminus of $RHAU_{53-105}$ is involved in binding to the G-quadruplex. The N-terminus of the RHAU construct was identified by superposition of the low resolution models calculated from the SAXS data for $RHAU_{53-105}$ and $RHAU_{53-150}$. Moreover, the low resolution model of the complex of hTR_{1-20} and $RHAU_{53-105}$ suggests that G-tetrad and not the sugar phosphate backbone of the quadruplex likely participates in the binding to $RHAU5_{3-105}$.[81]

The N-terminal construct of the RHAU protein was used in this analysis in order to study the binding between RHAU and the DNA analog of its quadruplex target formed by the hTR_{1-20} sequence. $RHAU_{53-105}$ was chosen because it contains the RSM motif (amino acids 54-66) previously shown to be required for quadruplex binding.[79] Moreover, CD spectra show that the construct possesses defined secondary structure. Although the full length RHAU has appreciably higher affinity for hTR_{1-20} than $RHAU_{53-105}$, the N-terminal construct was

nevertheless shown to bind hTR_{1-20} and hTR_{1-20} DNA by EMSA.[57,81] In addition, His_6-tagged-$RHAU_{53-105}$ was able to bind hTR in cell lysate depleted of endogenous full length RHAU, suggesting that the chosen construct is physiologically relevant.[81]

Additionally, expression of $RHAU_{53-1008}$ was attempted in *E.coli* strain BL21(DE3) supplemented with rare *E.coli* codons, but purification of the protein by affinity chromatography was unsuccessful and evidence of aggregation was detected. Since RHAU is a fairly large human protein, it might be better suited for expression in eukaryotic rather than in bacterial cells. For this purpose, His_6-$RHAU_{53-1008}^{\Delta 14}$ was cloned into the pCEP-Pu.BM40 vector optimized for overexpression of proteins in HEK293T cells. Moreover, HEK293T cells produce post-translational modifications not possible in *E. coli*, but which might nevertheless be physiologically relevant. Further research should in part focus on production and crystallization of full length RHAU protein.

A comprehensive biophysical approach was used to characterize the complex formed between DNA analogs of hTR_{1-20} and an N-terminal construct of RHAU. The findings presented here confirm and further describe the previously established interaction between RHAU and hTR_{1-20} DNA and compare the hydrodynamic parameters of the hTR_{1-20}·$RHAU_{53-105}$ complex to the complex of $RHAU_{53-105}$ with the hTR_{1-20} quadruplex DNA analog. Since the RSM of RHAU appears to interact with hTR1-20 and hTR1-20 DNA analogs in identical manner, it is worthwhile to pursue the attainment of the high resolution structure of the DNA complex. A high resolution structure depicting the $RHAU_{53-105}$·hTR_{1-20} DNA interaction is required to provide further insight into RHAU-quadruplex binding. Equally important, a high resolution structure of the full-length RHAU protein would yield new understanding of the mechanism of quadruplex unwinding by DEAH-box helicases.

In order to determine suitable crystallization conditions for hTR_{1-20} DNA, G-quadruplexes and their complexes with $RHAU_{53-105}$, several commercial crystallization screening kits from Hampton Research (CA, USA) were tested. Although neither hTR_{1-20} DNA_{c1} nor hTR_{1-20} DNA_{c1}·$RHAU_{53-105}$ crystallized in any of the screened solutions, crystals of hTR_{1-20} DNA_{c2}·$RHAU_{53-105}$ were obtained in 0.2 M sodium formate, 20 % w/v PEG 3350. These crystals diffracted X-rays weakly, but they also had the tendency to dissociate into parallel fine needle-like crystals unsuitable for good quality X-ray diffraction collection upon removal from the crystallization drop. Substitution of sodium with either potassium or ammonium also yielded hTR_{1-20} DNA_{c2}·$RHAU_{53-105}$ crystals that behaved similarly. An attempt to optimize this condition by varying the concentration of PEG 3350, pH and nature of the cation in the salt component of the crystallization solution failed to produce any usable crystals. However, in a subsequent screen for crystallization of hTR_{1-20} DNA_{c2}·$RHAU_{53-105}$, 1.5 M sodium chloride with 10 % v/v ethanol was revealed as a promising condition. Crystals that appeared two weeks after the screens were set-up absorbed methyl blue, suggesting that protein was present in them. This finding confirms that the observed crystals were not composed purely of salt. One crystal was tested for X-ray diffraction and was found to diffract X-rays weakly. Close examination of the crystal and its X-ray diffraction pattern suggests that it is composed of multiple microcrystals. Optimization of the 1.5 M sodium chloride with 10 % v/v ethanol condition is necessary. Furthermore, fine needle-like crystals were obtained for hTR_{1-20} DNA_{c2} in 0.4 M potassium sodium tartrate tetrahydrate, but they were too fine to measure for X-ray diffraction. Due to limited availability of hTR_{1-20} DNA, this condition was not optimized. Several promising condition for crystallization of hTR_{1-20} DNA_{c2} in complex with the N-terminal domain of the RHAU protein have been identified and are in need of further optimization. The N-terminal

domain investigated here is unique to RHAU and a high resolution structure of hTR_{1-20} DNA_{c2}·$RHAU_{53-105}$ is anticipated for the input it might provide into the understanding of the interaction between the RSM motif of RHAU and G-quadruplex oligonucleotides.

5. Summary and Future Directions

G-quadruplexes are thermodynamically stable secondary structures that have the propensity to form within guanine-rich single stranded polynucleotides. G-quadruplexes consist of consecutive guanine tetrads associated into ring-like structures through Hoogsteen hydrogen bonds that stack on top of each other. G-quadruplex structures have been identified within telomeres, promoter regions of genes, 5' and 3' UTRs of mRNAs and implicated in transcriptional and translational control. Since G-quadruplexes have been shown to act as *cis*-regulatory element within the genome and formation of aberrant G-quadruplexes within single-stranded regions of DNA has been associated with disease, it is wise to investigate the mechanisms of G-quadruplex recognition and unwinding by specialized helicases. RHAU, which has been identified as a protein that binds and unwinds a G-quadruplex in the 5' terminus of hTR, is a major source of G-quadruplex resolving activity in human cell lysates. The RSM region within the N-terminal domain of RHAU is responsible for recognition of G-quadruplexes by RHAU.

The binding between the DNA analog of hTR_{1-20} and the N-terminus of RHAU, $RHAU_{53-105}$, was studied using biophysical methods. Gel electrophoresis, UV-visible spectroscopy, spectropolarimetry, dynamic light scattering and small angle X-ray scattering were used to conduct a comprehensive analysis of hTR_{1-20} DNA, $RHAU_{53-105}$ and their complexes. The data show that hTR_{1-20} DNA assumes two conformations in the presence of potassium ions in solution. Moreover, both conformations of hTR_{1-20} assume parallel G-quadruplex secondary structure characterized by a disk-like shape with two concave faces. Formation of G-quadruplex is confirmed by staining with G-quadruplex specific dye N-Methylmesoporphyrin IX, significant hypochromicity at 297 nm at 80 °C relative to 20 °C, circular dichroism spectra with

characteristic minima and maxima at 242 and 263 nm, respectively, as well as estimated melting temperatures of ~70 °C for hTR_{1-20} DNA_{c1} and ~64 °C for hTR_{1-20} DNA_{c2}. Further, CD polarimetry and SAXS demonstrate that $RHAU_{53-105}$ assumes an extended (D_{max} = 7.8 nm , r_G = 2.1 (±0.2) nm) and ordered conformation in solution. Electrophoretic mobility shift assays show that $RHAU_{53-105}$ shifts both hTR_{1-20} DNA_{c1} and hTR_{1-20} DNA_{c2}. Complex formation between $RHAU_{53-105}$ and hTR_{1-20} DNA was further confirmed by spectropolarimetry, dynamic light scattering and SAXS. The low resolution SAXS models for the complexes appear more compact than the extended model for $RHAU_{53-105}$ construct (D_{max} = 5.0 nm for complex with hTR_{1-20} DNA_{c1}; D_{max} = 5.2 nm for complex with hTR_{1-20} DNA_{c2}; D_{max} = 7.8 nm $RHAU_{53-105}$ alone). CD spectra of the complexes are dominated by the G-quadruplex component beyond 250 nm, suggesting that hTR_{1-20} retains its G-quadruplex structure upon binding with $RHAU_{53-105}$. These findings characterize hTR_{1-20} DNA, $RHAU_{53-105}$ and their complexes, although a high resolution structure of the complex is required for a more specific elucidation of the this interaction. Currently, there is an ongoing attempt to crystallize the complex of $RHAU_{53-105}$ and hTR_{1-20} DNA_{c2} in order to obtain a high resolution structure of this complex by X-ray diffraction. Two conditions, 0.2 M sodium formate, 20 % (w/v) PEG 3350 and 1.5 M sodium chloride, 10 % (v/v) ethanol have been identified as suitable solutions for crystallization of hTR_{1-20} DNA_{c2}·$RHAU_{53-105}$, but further optimization of these conditions is necessary. In addition, the gene for the full-length RHAU protein was cloned into the pCEP-Pu.BM40 vector to be used in expression of RHAU in HEK293T cells. Purification and analysis of the full length RHAU protein alone and in complex with hTR would contribute toward the understanding of the mechanisms involved in G-quadruplex binding and unwinding.

6. References

(1) Laughlan, G., Murchie, a I., Norman, D. G., Moore, M. H., Moody, P. C., Lilley, D. M., and Luisi, B. (1994) The high-resolution crystal structure of a parallel-stranded guanine tetraplex. *Science 265*, 520–4.

(2) Phillips, K., Dauter, Z., Murchie, A. I. H., Lilley, D. M. J., and Luisi, B. (1997) The Crystal Structure of a parallel-stranded guanine tetraplex at 0 . 95 Å resolution. *J. Mol. Biol.273*, 171-182.

(3) Parkinson, G. N., Lee, M. P. H., and Neidle, S. (2002) Crystal structure of parallel quadruplexes from human telomeric DNA *417*, 3–7.

(4) Clark, G. R., Pytel, P. D., Squire, C. J., and Neidle, S. (2003) Structure of the first parallel DNA quadruplex-drug complex. *J. Am. Chem. Soc. 125*, 4066–7.

(5) Bugaut, A., and Balasubramanian, S. (2012) 5'-UTR RNA G-quadruplexes: translation regulation and targeting. *Nucleic Acids Res. 40*, 4727–41.

(6) Raiber, E.-A., Kranaster, R., Lam, E., Nikan, M., and Balasubramanian, S. (2012) A non-canonical DNA structure is a binding motif for the transcription factor SP1 in vitro. *Nucleic Acids Res. 40*, 1499–508.

(7) Martadinata, H., and Phan, A. T. (2014) Formation of a stacked dimeric G-quadruplex containing bulges by the 5'-terminal region of human telomerase RNA (hTERC). *Biochemistry 53*, 1595–600.

(8) Wang, Y., and Patel, D. J. (1993) Solution structure of the human telomeric repeat d[AG3(T2AG3)3] G-tetraplex. *Structure 1*, 263–82.

(9) Haider, S., Parkinson, G. N., and Neidle, S. (2002) Crystal structure of the potassium form of an *Oxytricha nova* G-quadruplex. *J. Mol. Biol. 320*, 189–200.

(10) Haider, S. M., Parkinson, G. N., and Neidle, S. (2003) Structure of a G-quadruplex–Ligand Complex. *J. Mol. Biol. 326*, 117–125.

(11) Nicoludis, J. M., Miller, S. T., Je, P. D., Barrett, S. P., Rablen, P. R., Lawton, T. J., and Yatsunyk, L. A. (2012) Optimized end-Seacking epovides specificity of N - methyl mesoporphyrin IX for human telomeric G-quadruplex DNA. *J. Am. Chem. Soc. 134*, 20446-20456.

(12) Wei, D., Parkinson, G. N., Reszka, A. P., and Neidle, S. (2012) Crystal structure of a c-kit promoter quadruplex reveals the structural role of metal ions and water molecules in maintaining loop conformation. *Nucleic Acids Res. 40*, 4691–700.

(13) Bazzicalupi, C., Ferraroni, M., Bilia, A. R., Scheggi, F., and Gratteri, P. (2013) The crystal structure of human telomeric DNA complexed with berberine: an interesting case of stacked ligand to G-tetrad ratio higher than 1:1. *Nucleic Acids Res. 41*, 632–8.

(14) Ding, D., Zhou, J., Wang, M., and Cong, Y. (2013) Implications of telomere-independent activities of telomerase reverse transcriptase in human cancer *280*, 3205–3211.

(15) Martadinata, H. (2014) Formation of a stacked dimeric G - quadruplex containing bulges by the 5 ′-terminal region of human telomerase RNA (hTERC). *Biochemistry 53*, 1595-1600.

(16) Morris, M. J., Negishi, Y., Pazsint, C., and Schonhoft, J. D. (2010) An RNA G-quadruplex is essential for cap-independent translation initiation in human VEGF IRES. *J. Am. Chem. Soc. 132*, 17831–17839.

(17) Martadinata, H., and Phan, A. T. (2013) Structure of human telomeric RNA (TERRA): stacking of two G-quadruplex blocks in K(+) solution. *Biochemistry 52*, 2176–83.

(18) Biffi, G., Tannahill, D., Mccafferty, J., and Balasubramanian, S. (2013) Quantitative visualization of DNA G-quadruplex structures in human cells. *Nat. Chem. 5*, 182–186.

(19) Biffi, G., Di Antonio, M., Tannahill, D., and Balasubramanian, S. (2014) Visualization and selective chemical targeting of RNA G-quadruplex structures in the cytoplasm of human cells. *Nat. Chem. 6*, 75–80.

(20) Maizels, N., and Gray, L. T. (2013) The G4 genome. *PLoS Genet. 9*, e1003468.

(21) Huppert, J. L., and Balasubramanian, S. (2005) Prevalence of quadruplexes in the human genome *33*, 2908–2916.

(22) Eddy, J., and Maizels, N. (2006) Gene function correlates with potential for G4 DNA formation in the human genome. *Nucleic Acids Res. 34*, 3887–3896.

(23) Halder, R., Halder, K., Sharma, P., and Garg, G. (2010) Guanine quadruplex DNA structure restricts methylation of CpG dinucleotides genome-wide. *Mol. BioSyst. 6*, 2439–2447.

(24) Huppert, J. L., and Balasubramanian, S. (2007) G-quadruplexes in promoters throughout the human genome *35*, 406–413.

(25) Siddiqui-jain, A., Grand, C. L., Bearss, D. J., and Hurley, L. H. (2002) Direct evidence for a G-quadruplex in a promoter region and its targeting with a small molecule to repress c-MYC transcription. *Proc. Natl. Acad. Sci. 99*, 11593–11598.

(26) Kumari, S., Bugaut, A., Huppert, J. L., and Balasubramanian, S. (2007) An RNA G-quadruplex in the 5’ UTR of the NRAS proto-oncogene modulates translation. *Nat. Chem. Biol. 3*, 218–21.

(27) Arora, A., Dutkiewicz, M., and Scaria, V. (2008) Inhibition of translation in living eukaryotic cells by an RNA G-quadruplex motif. *RNA 14*, 1290–1296.

(28) Gomez, D., Lemarteleur, T., Lacroix, L., Mailliet, P., Mergny, J.-L., and Riou, J.-F. (2004) Telomerase downregulation induced by the G-quadruplex ligand 12459 in A549 cells is mediated by hTERT RNA alternative splicing. *Nucleic Acids Res. 32*, 371–9.

(29) Sagne, C., Marcel, V., Bota, M., Martel-Planche, G., Nobrega, A., Palmero, E. I., Perriaud, L., Boniol, M., Vagner, S., Cox, D. G., Chan, C. S., Mergny, J.-L., Olivier, M., Ashton-Prolla, P., Hall, J., Hainaut, P., and Achatz, M. I. (2014) Age at cancer onset in germline TP53 mutation carriers: association with polymorphisms in predicted G-quadruplex structures. *Carcinogenesis 35*, 807–15.

(30) Bonnal, S., Schaeffer, C., Créancier, L., Clamens, S., Moine, H., Prats, A.-C., and Vagner, S. (2003) A single internal ribosome entry site containing a G quartet RNA structure drives fibroblast growth factor 2 gene expression at four alternative translation initiation codons. *J. Biol. Chem. 278*, 39330–6.

(31) Blackburn, E. H. (2005) Telomeres and telomerase: their mechanisms of action and the effects of altering their functions. *FEBS Lett. 579*, 859–62.

(32) Colgin, L. M., and Reddel, R. R. (1999) Telomere maintenance mechanisms and cellular immortalization. *Curr. Opin. Genet. Dev. 9*, 97–103.

(33) Yu, H.-Q., Miyoshi, D., and Sugimoto, N. (2006) Characterization of Structure and Stability of Long Telomeric DNA G-Quadruplexes. *J. Am. Chem. Soc. 128*, 15461–15468.

(34) Sarkies, P., Murat, P., Phillips, L. G., Patel, K. J., Balasubramanian, S., and Sale, J. E. (2012) FANCJ coordinates two pathways that maintain epigenetic stability at G-quadruplex DNA. *Nucleic Acids Res. 40*, 1485–98.

(35) Lormand, J. D., Buncher, N., Murphy, C. T., Kaur, P., Lee, M. Y., Burgers, P., Wang, H., Kunkel, T. a, and Opresko, P. L. (2013) DNA polymerase δ stalls on telomeric lagging strand templates independently from G-quadruplex formation. *Nucleic Acids Res. 41*, 10323–33.

(36) Dna, G., Sun, H., Karow, J. K., Hickson, I. D., and Maizels, N. (1998) The bloom's syndrome helicase unwinds G4 DNA. *J. Biol. Chem. 42*, 27587-27592.

(37) Fry, M., and Loeb, L. A. (1999) Human werner syndrome DNA helicase unwinds tetrahelical structures of the Fragile X syndrome repeat sequence d(CGG)n structures of the Fragile X syndrome repeat sequence d(CGG)$_n$. *J. Biol. Chem. 274*, 12979-12802.

(38) London, T. B. C., Barber, L. J., Mosedale, G., Kelly, G. P., Balasubramanian, S., Hickson, I. D., Boulton, S. J., and Hiom, K. (2008) FANCJ is a structure-specific DNA helicase associated with the maintenance of genomic G/C tracts. *J. Biol. Chem. 283*, 36132–9.

(39) Fratta, P., Mizielinska, S., Nicoll, A. J., Zloh, M., Fisher, E. M. C., Parkinson, G., and Isaacs, A. M. (2012) C9orf72 hexanucleotide repeat associated with amyotrophic lateral sclerosis and frontotemporal dementia forms RNA G-quadruplexes. *Sci. Rep. 2*, 1016.

(40) Haeusler, A. R., Donnelly, C. J., Periz, G., Simko, E. a J., Shaw, P. G., Kim, M.-S., Maragakis, N. J., Troncoso, J. C., Pandey, A., Sattler, R., Rothstein, J. D., and Wang, J. (2014) C9orf72 nucleotide repeat structures initiate molecular cascades of disease. *Nature 507*, 195–200.

(41) DeJesus-Hernandez, M., Mackenzie, I. R., Boeve, B. F., Boxer, A. L., Baker, M., Rutherford, N. J., Nicholson, A. M., Finch, N. a, Flynn, H., Adamson, J., Kouri, N., Wojtas, A., Sengdy, P., Hsiung, G.-Y. R., Karydas, A., Seeley, W. W., Josephs, K. a, Coppola, G., Geschwind, D. H., Wszolek, Z. K., Feldman, H., Knopman, D. S., Petersen, R. C., Miller, B. L., Dickson, D. W., Boylan, K. B., Graff-Radford, N. R., and Rademakers, R. (2011) Expanded GGGGCC hexanucleotide repeat in noncoding region of C9ORF72 causes chromosome 9p-linked FTD and ALS. *Neuron 72*, 245–56.

(42) Wu, Y., Shin-ya, K., and Brosh, R. M. (2008) FANCJ helicase defective in Fanconia anemia and breast cancer unwinds G-quadruplex DNA to defend genomic stability. *Mol. Cell. Biol. 28*, 4116–28.

(43) Han, H., and Hurley, L. H. (2000) G-quadruplex DNA: a potential target for anti-cancer drug design. *TiPS 21*, 136–142.

(44) Tran, H., Schilling, M., Wirbelauer, C., Hess, D., and Nagamine, Y. (2004) Facilitation of mRNA deadenylation and decay by the exosome-bound , DExH protein RHAU. *Mol. Cell 13*, 101–111.

(45) Kim, H., Lee, J., Bae, S., Ryoo, H., Kim, H., Ha, H., and Lee, Z. H. (2011) Histone deacetylase inhibitor MS-275 stimulates bone transcription. *J. Bone Miner. Res 26*, 2161–2173.

(46) Huang, W., Smaldino, P. J., Zhang, Q., Miller, L. D., Cao, P., Stadelman, K., Wan, M., Giri, B., Lei, M., Nagamine, Y., Vaughn, J. P., Akman, S. a, and Sui, G. (2012) Yin Yang 1 contains G-quadruplex structures in its promoter and 5'-UTR and its expression is modulated by G4 resolvase 1. *Nucleic Acids Res. 40*, 1033–49.

(47) Lai, J. C., Ponti, S., Pan, D., Kohler, H., Skoda, R. C., Matthias, P., and Nagamine, Y. (2012) The DEAH-box helicase RHAU is an essential gene and critical for mouse hematopoiesis. *Blood 119*, 4291–300.

(48) Iwamoto, F., Stadler, M., Chalupníková, K., Oakeley, E., and Nagamine, Y. (2008) Transcription-dependent nucleolar cap localization and possible nuclear function of DExH RNA helicase RHAU. *Exp. Cell Res. 314*, 1378–91.

(49) Chalupníková, K., Lattmann, S., Selak, N., Iwamoto, F., Fujiki, Y., and Nagamine, Y. (2008) Recruitment of the RNA helicase RHAU to stress granules via a unique RNA-binding domain. *J. Biol. Chem. 283*, 35186–98.

(50) Booy, E. P., Howard, R., Marushchak, O., Ariyo, E. O., Meier, M., Novakowski, S. K., Deo, S. R., Dzananovic, E., Stetefeld, J., and McKenna, S. a. (2014) The RNA helicase RHAU (DHX36) suppresses expression of the transcription factor PITX1. *Nucleic Acids Res. 42*, 3346–61.

(51) Bicker, S., Khudayberdiev, S., Weiß, K., Zocher, K., Baumeister, S., and Schratt, G. (2013) The DEAH-box helicase DHX36 mediates dendritic localization of the neuronal precursor-microRNA-134. *Genes Dev. 27*, 991–6.

(52) Vaughn, J. P., Creacy, S. D., Routh, E. D., Joyner-Butt, C., Jenkins, G. S., Pauli, S., Nagamine, Y., and Akman, S. a. (2005) The DEXH protein product of the DHX36 gene is the major source of tetramolecular quadruplex G4-DNA resolving activity in HeLa cell lysates. *J. Biol. Chem. 280*, 38117–20.

(53) Creacy, S. D., Routh, E. D., Iwamoto, F., Nagamine, Y., Akman, S. a, and Vaughn, J. P. (2008) G4 resolvase 1 binds both DNA and RNA tetramolecular quadruplex with high affinity and is the major source of tetramolecular quadruplex G4-DNA and G4-RNA resolving activity in HeLa cell lysates. *J. Biol. Chem. 283*, 34626–34.

(54) Giri, B., Smaldino, P. J., Thys, R. G., Creacy, S. D., Routh, E. D., Hantgan, R. R., Lattmann, S., Nagamine, Y., Akman, S. A., and Vaughn, J. P. (2011) G4 Resolvase 1 tightly binds and unwinds unimolecular G4-DN. *Nucleic Acids. Res 39*, 7161–7178.

(55) Lattmann, S., Stadler, M. B., Vaughn, J. P., Akman, S. A., and Nagamine, Y. (2011) The DEAH-box RNA helicase RHAU binds an intramolecular RNA G-quadruplex in TERC and associates with telomerase holoenzyme. *Nucleic Acids Res. 39*, 9390–9404.

(56) Sexton, A. N., and Collins, K. (2011) The 5' guanosine tracts of human telomerase RNA are recognized by the G-quadruplex binding domain of the RNA helicase DHX36 and function to increase RNA accumulation. *Mol. Cell. Biol. 31*, 736–43.

(57) Booy, E. P., Meier, M., Okun, N., Novakowski, S. K., Xiong, S., Stetefeld, J., and McKenna, S. a. (2012) The RNA helicase RHAU (DHX36) unwinds a G4-quadruplex in human telomerase RNA and promotes the formation of the P1 helix template boundary. *Nucleic Acids Res. 40*, 4110–24.

(58) Chen, J. L., Blasco, M. a, and Greider, C. W. (2000) Secondary structure of vertebrate telomerase RNA. *Cell 100*, 503–14.

(59) Chen, J.-L., and Greider, C. W. (2003) Template boundary definition in mammalian telomerase. *Genes Dev. 17*, 2747–52.

(60) Gros, J., Guédin, A., Mergny, J.-L., and Lacroix, L. (2008) G-Quadruplex formation interferes with P1 helix formation in the RNA component of telomerase hTERC. *Chembiochem 9*, 2075–9.

(61) Lacroix, L., Séosse, A., and Mergny, J.-L. (2011) Fluorescence-based duplex-quadruplex competition test to screen for telomerase RNA quadruplex ligands. *Nucleic Acids Res. 39*, e21.

(62) Guex, N., Peitsch, M. C., and Schwede, T. (2009) Automated comparative protein structure modeling with SWISS-MODEL and Swiss-PdbViewer: a historical perspective. *Electrophoresis 30 Suppl 1*, S162–73.

(63) Kiefer, F., Arnold, K., Künzli, M., Bordoli, L., and Schwede, T. (2009) The SWISS-MODEL Repository and associated resources. *Nucleic Acids Res. 37*, D387–92.

(64) Arnold, K., Bordoli, L., Kopp, J., and Schwede, T. (2006) The SWISS-MODEL workspace: a web-based environment for protein structure homology modelling. *Bioinformatics 22*, 195–201.

(65) Biasini, M., Bienert, S., Waterhouse, A., Arnold, K., Studer, G., Schmidt, T., Kiefer, F., Cassarino, T. G., Bertoni, M., Bordoli, L., and Schwede, T. (2014) SWISS-MODEL: modelling protein tertiary and quaternary structure using evolutionary information. *Nucleic Acids Res.* 1–7.

(66) Büttner, K., Nehring, S., and Hopfner, K.-P. (2007) Structural basis for DNA duplex separation by a superfamily-2 helicase. *Nat. Struct. Mol. Biol. 14*, 647–52.

(67) Pyle, A. M. (2008) Translocation and unwinding mechanisms of RNA and DNA helicases. *Annu. Rev. Biophys. 37*, 317-336.

(68) Walbott, H., Mouffok, S., Capeyrou, R., Lebaron, S., Humbert, O., van Tilbeurgh, H., Henry, Y., and Leulliot, N. (2010) Prp43p contains a processive helicase structural architecture with a specific regulatory domain. *EMBO J. 29*, 2194–204.

(69) Schütz, P., Wahlberg, E., Karlberg, T., Hammarström, M., Collins, R., Flores, A., and Schüler, H. (2010) Crystal structure of human RNA helicase A (DHX9): structural basis for unselective nucleotide base binding in a DEAD-box variant protein. *J. Mol. Biol. 400*, 768–82.

(70) Weir, J. R., Bonneau, F., Hentschel, J., and Conti, E. (2010) Structural analysis reveals the characteristic features of Mtr4, a DExH helicase involved in nuclear RNA processing and surveillance. *Proc. Natl. Acad. Sci. U. S. A. 107*, 12139–44.

(71) Halbach, F., Rode, M., and Conti, E. (2012) The crystal structure of S. cerevisiae Ski2, a DExH helicase associated with the cytoplasmic functions of the exosome. *RNA 18*, 124–34.

(72) Wilkins, M. R., Gasteiger, E., Bairoch, a, Sanchez, J. C., Williams, K. L., Appel, R. D., and Hochstrasser, D. F. (1999) Protein identification and analysis tools in the ExPASy server. *Methods Mol. Biol. 112*, 531–52.

(73) Svergun, D. I. (1992) Determination of the regularization parameter in indirect-transform methods using perceptual criteria. *J. Appl. Crystallogr. 25*, 495–503.

(74) Svergun, D. I. (1999) Restoring low resolution structure of biological macromolecules from solution scattering using simulated annealing. *Biophys. J. 76*, 2879–86.

(75) Volkov, V. V, and Svergun, D. I. (2003) Uniqueness of ab initio shape determination in small-angle scattering. *J. Appl. Crystallogr. 36*, 860–864.

(76) García De La Torre, J., Huertas, M. L., and Carrasco, B. (2000) Calculation of hydrodynamic properties of globular proteins from their atomic-level structure. *Biophys. J. 78*, 719–30.

(77) Brahms, S., and Brahms, J. (1980) Determination of protein secondary structure in solution by vacuum ultraviolet circular dichroism. *J. Mol. Biol. 138*, 149–78.

(78) Huppert, J. L., Bugaut, A., Kumari, S., and Balasubramanian, S. (2008) G-quadruplexes: the beginning and end of UTRs. *Nucleic Acids Res. 36*, 6260–6268.

(79) Lattmann, S., Giri, B., Vaughn, J. P., Akman, S. A., and Nagamine, Y. (2010) Role of the amino terminal RHAU-specific motif in the recognition and resolution of guanine quadruplex-RNA by the DEAH-box RNA helicase RHAU. *Nucleic Acids Res. 38*, 6219–6233.

(80) Olsen, C. M., Lee, H.-T., and Marky, L. a. (2009) Unfolding thermodynamics of intramolecular G-quadruplexes: base sequence contributions of the loops. *J. Phys. Chem. B 113*, 2587–95.

(81) Meier, M., Patel, T. R., Booy, E. P., Marushchak, O., Okun, N., Deo, S., Howard, R., McEleney, K., Harding, S. E., Stetefeld, J., and McKenna, S. a. (2013) Binding of G-quadruplexes to the N-terminal recognition domain of the RNA helicase associated with AU-rich element (RHAU). *J. Biol. Chem. 288*, 35014–27.

(82) Burge, S., Parkinson, G. N., Hazel, P., Todd, A. K., and Neidle, S. (2006) Quadruplex DNA: sequence , topology and structure. *Nucleic Acids Res. 34*, 5402–5415.

(83) Sauerwald, A., Sandin, S., Cristofari, G., Scheres, S. H. W., Lingner, J., and Rhodes, D. (2013) Structure of active dimeric human telomerase. *Nat. Struct. Mol. Biol. 20*, 454–60.

7. Appendix

7.1 LIST OF ABBREVIATIONS

ALS	Amyotrophic lateral sclerosis
ATP	Adenosine triphosphate
ATR	Alternatively translated region
BLM	Bloom syndrome protein
CD	Circular dichroism
c-KYT	Gene that encodes tyrosine-protein kinase Kit protein
c-MYC	Gene that encodes transcription factor Myc
CR	Conserved region
DHX36	Alternative name for RHAU protein
DLS	Dynamic light scattering
D_{max}	Maximum particle dimension
DNA	Deoxyribonucleic acid
FANCJ	Faconi anemia group J protein
FGF-2	Fibroblast growth factor 2
FTD	Frontotemporal dementia
His_6	Hexahistidine
HRP	Horseradish peroxidase
hTERT	Human telomerase reverse transcriptase
hTR	Human telomerase reverse transcriptase RNA
HuR	Human antigen R
IPTG	β-D-1-thiogalactopyranoside
IRES	Internal ribosome entry site
LB	Luria broth
miRNA134	Micro-RNA-134
mRNA	Messenger RNA
NFAR1	Interleukin enhancer binding factor 3
NMM	N-methyl mesoporphyrin IX
NMR	Nuclear magnetic resonance
NRAS	Neuroblastoma RAS viral (v-ras) oncogene homolog
NSD	Normalized spatial discrepancy
P(r)	Electron pair distribution function
p53	Tumor protein 53
P68	P68 RNA Helicase, also known as DDX5
P72	P72 RNA Helicase, also known as DDX17
PARN	Polyadenylate-specific ribonucleases
PEG	Polyethylene glycol
PITX1	Paired-like homeodomain 1 protein
R_g	Radius of gyration
R_H	Radius of hydration
RHAU	RNA associated with *AU*-rich element
RNA	Ribonucleic acid
RSM	RHAU-specific motif

SAXS	Small angle X-ray scattering
SEC	Size exclusion chromatography
SDS-PAGE	Sodium dodecyl sulfate polyacrylamide gel electrophoresis
SF2	Superfamily2
TBE	Tris/Borate/EDTA (Ethylenediaminetetraacetic acid)
TERRA RNA	Telomeric non-coding ribonucleic acid
TERT	Catalytic component of telomerase reverse transcriptase holoenzyme
TNAP	Tissue-nonspecific alkaline phosphatase
TP53	Gene that encodes p53 protein
UTR	Untranslated region
UV-Vis	Ultraviolet-visisble
WRN	Werner protein
YY1	Yin Yang 1 protein
χ	Chi value